Resource

Developmental Cell

Gene regulatory networks shape developmental plasticity of root cell types under water extremes in rice

Graphical abstract

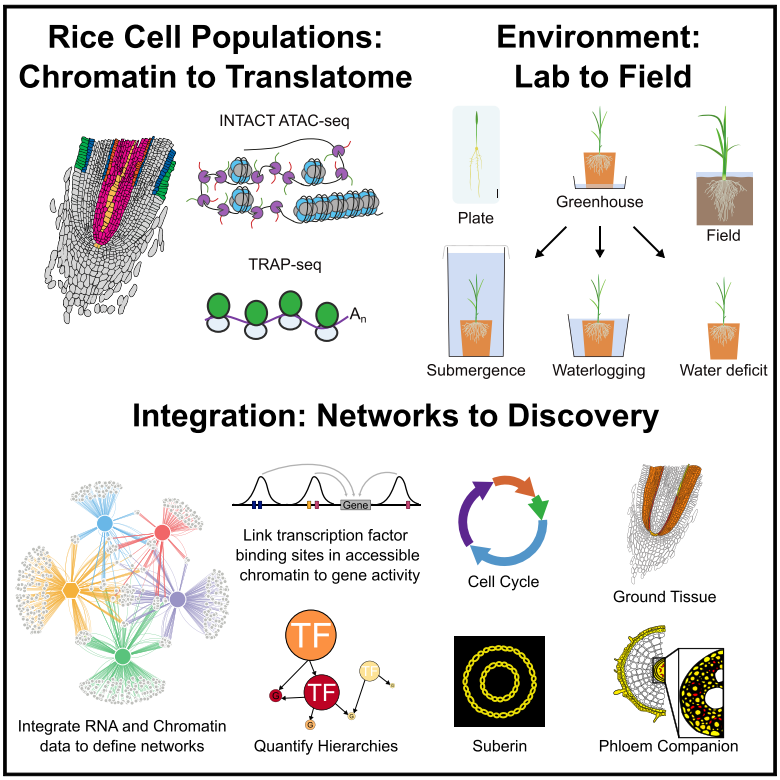

Highlights

- A translatome and chromatin atlas of rice root cell populations in nine environments
- Cell-type population signatures can be maintained or perturbed across environments
- Dynamic regulatory networks and transcription factor hierarchies of cell populations
- Conditional plasticity of the cell cycle and barrier cell suberization and Fe uptake

Authors

Mauricio A. Reynoso, Alexander T. Borowsky, Germain C. Pauluzzi, ..., Siobhan M. Brady, Thomas Girke, Julia Bailey-Serres

Correspondence

serres@ucr.edu

In brief

Reynoso, Borowsky, Pauluzzi, et al. provide an atlas of gene activity of root cell populations of rice in varied agronomically relevant environments. They identify genomic *cis*- and *trans*-regulatory factors involved in stress responses that can facilitate breeding and engineering climate-resilient crops.

Reynoso et al., 2022, Developmental Cell *57*, 1177–1192
May 9, 2022
https://doi.org/10.1016/j.devcel.2022.04.013

CellPress

Developmental Cell

CellPress
OPEN ACCESS

Resource

Gene regulatory networks shape developmental plasticity of root cell types under water extremes in rice

Mauricio A. Reynoso,[1,2,8] Alexander T. Borowsky,[1,8] Germain C. Pauluzzi,[1,8] Elaine Yeung,[1] Jianhai Zhang,[1] Elide Formentin,[1,3] Joel Velasco,[1] Sean Cabanlit,[1] Christine Duvenjian,[1] Matthew J. Prior,[1] Garo Z. Akmakjian,[1] Roger B. Deal,[4] Neelima R. Sinha,[5] Siobhan M. Brady,[6] Thomas Girke,[1] and Julia Bailey-Serres[1,7,9,*]

[1]Center for Plant Cell Biology, Department of Botany and Plant Sciences, University of California, Riverside, Riverside, CA 92521, USA
[2]IBBM, FCE-UNLP CONICET, La Plata 1900, Argentina
[3]Department of Biology, University of Padova, Padova, Italy
[4]Department of Biology, Emory University, Atlanta, GA 30322, USA
[5]Department of Plant Biology, University of California, Davis, Davis, CA 95616, USA
[6]Department of Plant Biology and Genome Center, University of California, Davis, Davis, CA 95616, USA
[7]Plant Ecophysiology, Institute of Environmental Biology, Utrecht University, 3584 Utrecht, the Netherlands
[8]These authors contributed equally
[9]Lead contact
*Correspondence: serres@ucr.edu
https://doi.org/10.1016/j.devcel.2022.04.013

SUMMARY

Understanding how roots modulate development under varied irrigation or rainfall is crucial for development of climate-resilient crops. We established a toolbox of tagged rice lines to profile translating mRNAs and chromatin accessibility within specific cell populations. We used these to study roots in a range of environments: plates in the lab, controlled greenhouse stress and recovery conditions, and outdoors in a paddy. Integration of chromatin and mRNA data resolves regulatory networks of the following: cycle genes in proliferating cells that attenuate DNA synthesis under submergence; genes involved in auxin signaling, the circadian clock, and small RNA regulation in ground tissue; and suberin biosynthesis, iron transporters, and nitrogen assimilation in endodermal/exodermal cells modulated with water availability. By applying a systems approach, we identify known and candidate driver transcription factors of water-deficit responses and xylem development plasticity. Collectively, this resource will facilitate genetic improvements in root systems for optimal climate resilience.

INTRODUCTION

Plants integrate environmental cues to balance energy use for growth versus survival strategies under intermittent water extreme stresses (Mickelbart et al., 2015). Roots are central to this perception. They develop from a stem cell niche into the longitudinal files of dividing cells that progressively differentiate to form radial layers of distinct cell types. Cells of these longitudinal files proliferate in the meristematic zone, expand in the elongation zone, and conclude differentiation in the maturation zone. The radial layers of rice (*Oryza sativa* L.) roots include the epidermis, ground tissue (exodermis, sclerenchyma, inner cortex, and endodermis), and vasculature (pericycle, phloem, and xylem). How cells of developmental zones of roots perceive and adjust to soil moisture fluctuations to benefit and sustain growth and survival is far from understood.

Here, we resolve patterns of gene activity in meristematic and differentiated root cell types of rice cultivated in a paddy or exposed to extremes in water availability. Soil moisture is a major determinant of architectural and anatomical traits of root systems. Many cultivars thrive in waterlogged (WL) anaerobic soils due to traits that enhance root aeration: shallow roots with gas passages within the cortical layer called aerenchyma and a apoplastic barrier on exodermal cell walls formed of the fatty acid polymer suberin, forming a barrier to radial loss of oxygen (Yamauchi et al, 2018). Rice is notable for its ability to endure complete submergence (SUB) by modulation of elongation growth; however, little is known of the effect of SUB on roots (Voesenek and Bailey-Serres, 2015; Yeung et al., 2019). By contrast to paddy varieties, rice cultivated in drier upland ecosystems develop deep and aerenchymatous roots to access moisture (Kadam et al., 2017; Lucob-Agustin et al., 2021; Uga et al., 2013). Sudden water deficiency activates abscisic acid (ABA) perception and response mechanisms that are well described for shoot tissues (Gupta et al., 2020). Trait plasticity involves transcriptional networks, wherein transcription factors (TFs) bind *cis*-regulatory DNA of target genes to regulate synthesis of mRNAs. Identification of the *cis*- and *trans*-regulatory factors

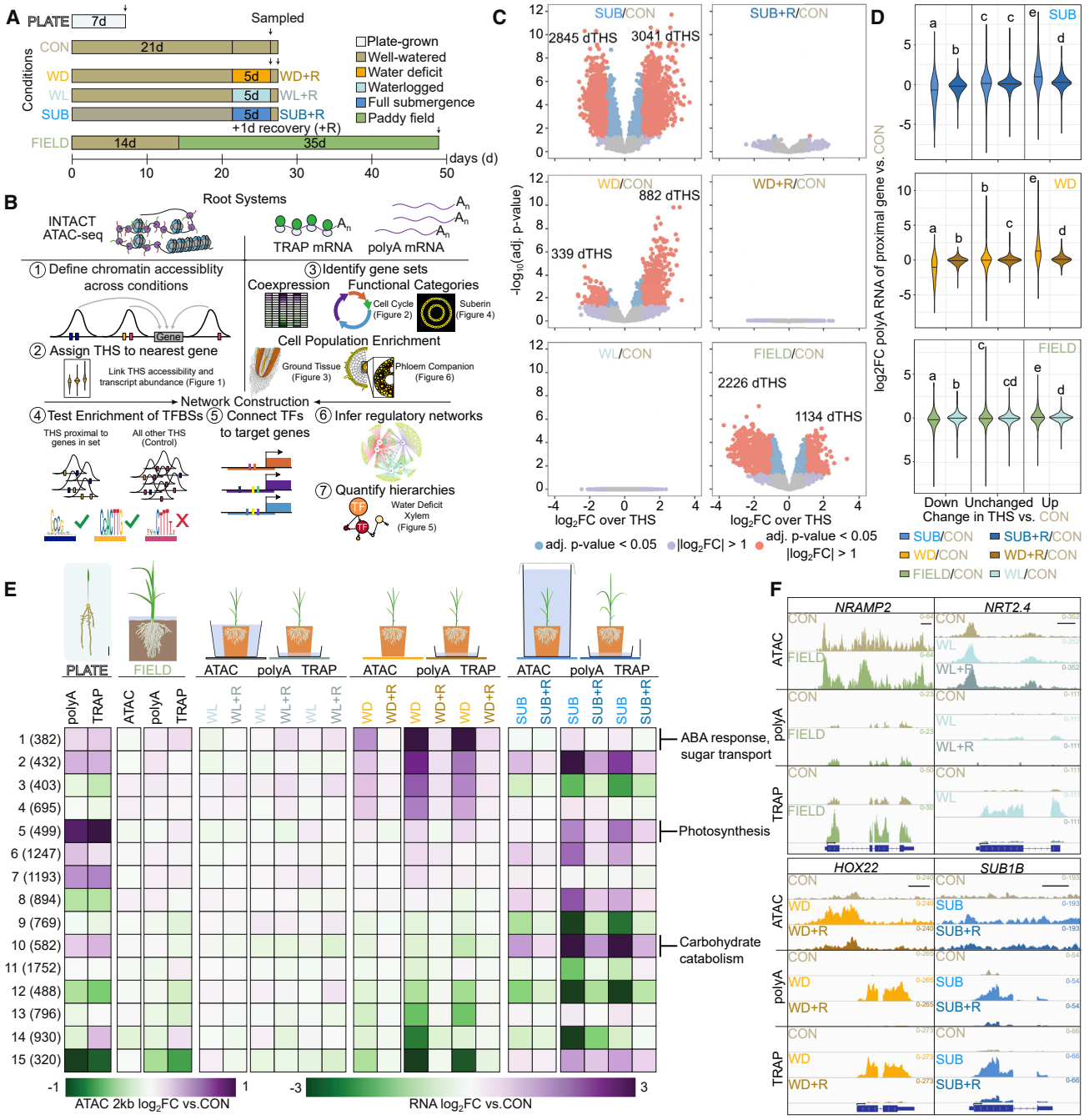

Figure 1. Chromatin accessibility and transcript abundance are coordinately and reversibly regulated in root systems of rice grown in diverse environments

(A) Overview of the ten growth conditions and treatments used in this study (detailed in Figure S1). Water sufficient and extreme treatments were performed on pot-grown plants.

(B) *p35S:INTACT* was used for nuclei capture to evaluate chromatin accessibility by ATAC-seq. *p35S:TRAP* was used for polyadenylated (polyA) mRNA-seq and translating ribosome affinity purification for TRAP-seq of polyadenylated ribosome-associated mRNAs. RNA abundance and chromatin accessibility based on transposase hypersensitive sites (THSs) were integrated in analyses surveying the presence of known TF motifs.

(C) Volcano plots demonstrate that significant changes in chromatin accessibility by water deficit (WD) and submergence (SUB) are reversed by 1 day poststress recovery (+1R). THSs are very similar in 5 days waterlogged (WL) relative to pot-grown control (well-watered) root systems (CON). Differential THSs (dTHSs) are distinguishable between pot- and field-grown roots.

(D) Violin plots demonstrate consistent up- or down-regulation of polyA RNA (log_2-fold change [FC]) for genes with significant upregulation or downregulation in chromatin accessibility over nearby THSs (padj [adjusted] < 0.05) by WD and SUB and recovery versus CON and in the field versus CON comparison. ANOVA was used to evaluate differences in mean log_2 FC; letters indicate groups in an LSD test.

(legend continued on next page)

that control the progression of development and metabolism in varied root environments can inform efforts to improve climate resilience of rice and other crops (Akmakjian and Bailey-Serres, 2022).

Using promoter-driven genetic tools, we gain insight into environmental regulation of development and metabolism in rice. To monitor chromatin accessibility, we paired the isolation of nuclei tagged in specific cell types (INTACT) with assay for transposase-accessible chromatin sequencing (ATAC-seq) (Buenrostro et al., 2013; Deal and Henikoff, 2010). To assess gene activity, we employed translating ribosome affinity purification-mRNA sequencing (TRAP-seq) (Juntawong et al., 2014). We established a collection of lines expressing near-constitutive and developmentally regulated promoters to drive INTACT and TRAP constructs. This enabled profiling of gene activity of roots of plants grown in pots under controlled conditions and in a paddy field. As accessible chromatin regions are associated with TF activity (Dorrity et al., 2021; Marand et al., 2021; Reynoso et al., 2019), we integrated our chromatin and mRNA data to assemble environmentally responsive gene regulatory modules of cell populations. Our results resolve how environment influences developmental programs of cell cohorts, including those undergoing division, differentiation, and modifications that facilitate aeration, water retention, and nutrient transport.

RESULTS

Environmental regulation of promoter accessibility is reversible and correlated with transcript dynamics

To broaden the perspective on environmental control of gene regulation, we assayed root systems of plants in nine conditions: grown on media, cultivated in a paddy field, or in the greenhouse and then exposed to sublethal water extremes (Figures 1A and S1A–S1C; Tables S1A and S1B). The environmental conditions included well-watered (CON), WL, complete SUB, or water deficit (WD) (Figure S1; Table S1). Response reversibility was monitored by sampling after one day of recovery: rewatering after WD (WD+R), drainage after WL (WL+R), and desubmergence (SUB+R). To establish a global view of the response signatures, we started with a *p35S:INTACT* line to monitor accessible chromatin by INTACT-ATAC-seq and a *p35S:TRAP* line to monitor the transcriptome and translatome and progressed to promoters that mark specific cell populations (Table S2). The domains of expression of these promoters were visualized by GFP or ß-glucuronidase (GUS) detection (Data S1). As each promoter may be conditionally regulated along with ribosome synthesis, we refer to each translatome monitored by the promoter name. Finally, we integrated the chromatin and gene activity information by testing the enrichment of TF binding sites (TFBSs) and inferring gene regulatory networks (Figure 1B).

ATAC-seq reads from rice roots predominantly map within 2 kb upstream of the transcription start site (TSS) of protein coding genes with high reproducibility (Figure S2A; Table S3A) and define regions of chromatin accessibility (transposase hypersensitive sites [THSs]) that are differentially regulated (dTHSs). WD and SUB, but not waterlogging, significantly modified chromatin accessibility (Figure 1C; Table S3B). The dTHSs generally reverse to prestress accessibility levels within 24 h of recovery. We found that chromatin accessibility is highly similar in well-watered or waterlogging roots, whereas roots of older field-grown plants have more closed than open chromatin regions compared with the roots of well-watered greenhouse plants (Figures 1C, S2B, and S2C). The growth environment similarly influences the transcriptome and translatome (Figure S2E).

To assess whether dynamics in chromatin accessibility are predictive of change in mRNA accumulation, we assigned each THS to the nearest gene in the genome. This confirms that the genes proximal (within 2 kb) to conditionally open THS (up-dTHS) are significantly more upregulated and genes proximal to closed THS (down-dTHS) are significantly more downregulated by water extremes (Figures 1D and S2D; Table S3C). This trend holds for dTHSs that are 2–12 kb from the nearest gene (Figure S2D). The changes in promoter chromatin accessibility coordinate with changes in steady-state and ribosome-bound mRNA abundance (Figure 1E; Table S4), as illustrated for genes induced by WD (cluster 1; includes ABA response and sugar transport genes) and SUB (cluster 10; includes carbohydrate catabolism genes), including signature conditionally expressed genes (Figure 1F). Light-responsive gene activity distinguishes plate-grown roots. As dynamics in chromatin accessibility and translated mRNA are coordinated for most clusters of coregulated genes (conditional ΔATAC versus ΔTRAP correlation: WD, R^2 = 0.91 and SUB, R^2 = 0.94; Figure S2F), we proceeded to integrate THS and translatome data to elucidate conditional gene regulatory dynamics of distinct cell populations.

Water extremes distinctly influence cell-cycle activity in roots

Root postembryonic development is orchestrated through the coordinated cell division and differentiation of cells in the meristematic root apex. In rice, modulation of cell division and differentiation facilitates growth responses to salt, WD, and seasonal floods (Lorbiecke and Sauter, 1999; Meguro and Sato, 2014; Nagai et al., 2020; Ogawa et al., 2011; Schuppler et al., 1998) but is unstudied in roots of WL or submerged plants. We used *pRSS1:TRAP*, expressed in proliferating cells (Figures 2A and S2), to contrast translatomes of dividing cells to those captured by *p35S:TRAP* in the environments surveyed (Figure S3A; Table S1B). Distinctions between the translatomes of the *pRSS1* and *p35S* cell populations are evident from grouping genes with similar conditional regulation using dominant pattern analysis (Orlando et al., 2009; Figure 2A; Tables S5A and S5B). mRNAs in the gene ontology (GO) category associated with

(E) Integrated cluster analysis of ATAC-seq and RNA abundance dynamics. Heatmap of $\log_2$ FC of differentially regulated transcripts ($|\log_2 FC| > 1$ and [padj < 0.01]) and $\log_2$ FC of chromatin accessibility within 2 kb upstream of transcript coding regions by WD, WL, SUB, or recovery (+1R, plate and field) growth for polyA and TRAP RNA. All comparisons are relative to pot-grown control (CON) root systems. Gene number in cluster in parenthesis. Selected significant gene ontology (GO) category enrichment indicated to provide biological context.

(F) Genome browser view of chromatin and transcript data for representative genes. Genes are oriented from 5′ to 3′. Scale bars, 0.5 kb. y-axis values are normalized TPM (RNA) or RPKM (ATAC).

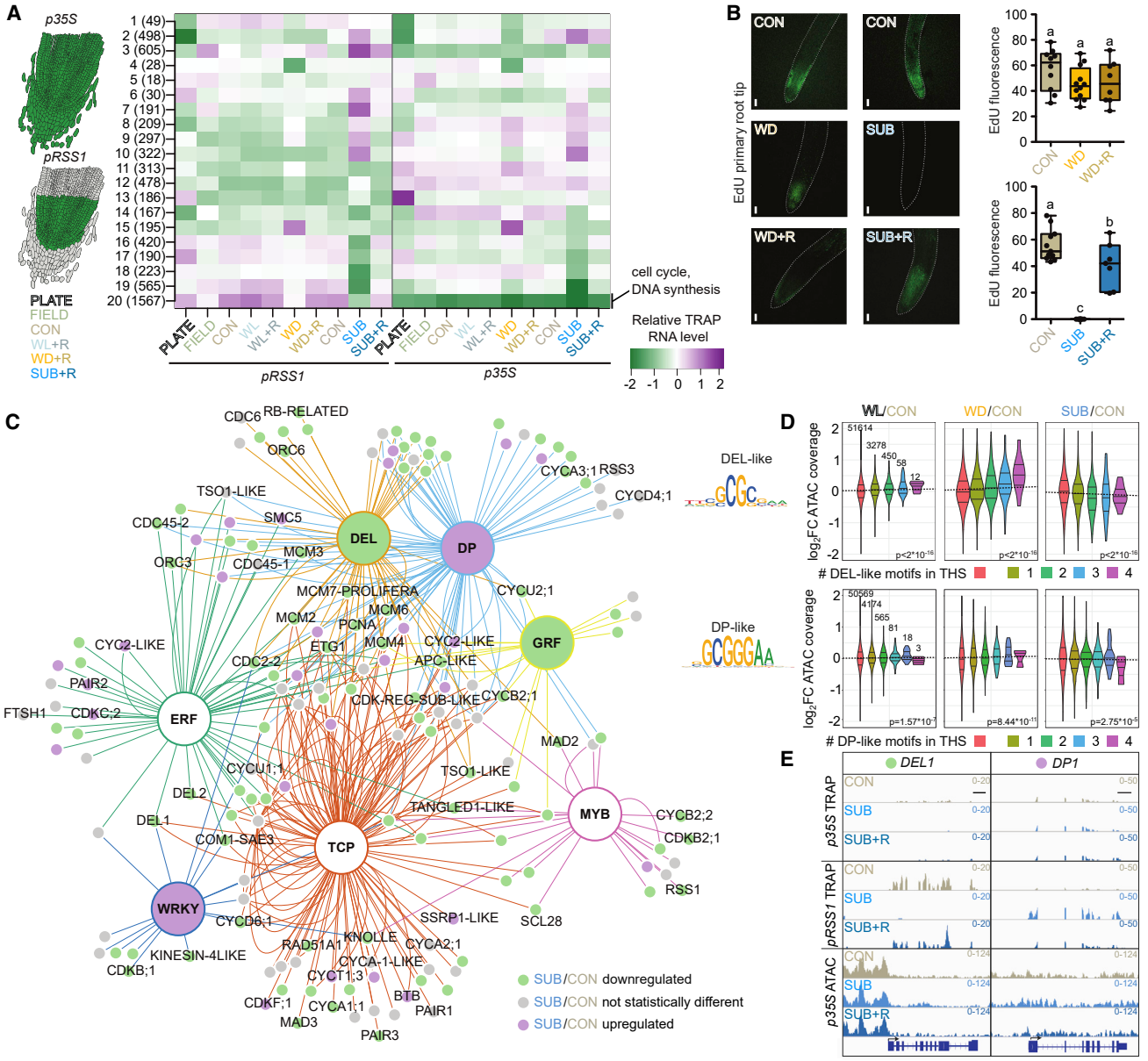

Figure 2. Water availability dynamically influences cell-cycle activity in roots

(A) Gene activity of dividing cells (*pRSS1:TRAP*) was compared with the broader root cell population (*p35S:TRAP*) by contrasting the translatomes under nine growth conditions. Heatmap of scaled TPM TRAP RNA levels for genes that show different accumulation organized by dominant pattern analysis. Pattern 20 is enriched for cell cycle (padj E−29) and DNA replication (padj E−29). Number of genes in pattern in parenthesis.

(B) Confocal images of EdU fluorescence of 8- to 11-day-old roots stained with 100 μM EdU for 1 h after treatment. Scale bars, 100 μm. Mean value of intensity at the elongation zone under SUB (n = 7–11 plants, 3 bioreps), WD (n = 8–12 plants, 3 bioreps), and following recovery. Letters represent significant differences ($p < 0.05$, one-way ANOVA analysis with multiple comparisons test).

(C) Network for regulation of cell cycle and DNA replication genes altered in *pRSS1* translatomes inferred from TFs that show enrichment in binding sites in THSs nearby (up to 2 kb/1 kb upstream/downstream).

(D) Change in chromatin accessibility in plants in WD, WL, and SUB versus control for THSs containing DEL-like or DP-like binding motifs. The p-value for each linear model is indicated.

(E) Root *p35S* ATAC-seq, *pRSS1* and *p35S* TRAP coverage under control, SUB and recovery for *OsDEL*-like and *DP-like* genes. Genes are oriented from 5′ to 3′. Scale bars, 0.5 kb. y-axis values are normalized TPM (RNA) or RPKM (ATAC).

water stress are upregulated and enriched in pattern 15 (padj E−8) in both *p35S* and *pRSS1* translatomes. mRNAs elevated by SUB are evident in one (*pRSS1*, pattern 3) or both translatomes (patterns 2, 6, 9, and 10). Similarly, accessibility of the proximal promoter region of these gene groups shows concordant conditional regulation (Figure S3B). *pRSS1*-expressing cells are strikingly enriched for ribosome-bound mRNAs in pattern 20 that contain GO terms for DNA replication (padj

E−29) and mitotic cell cycle (padj E−20). These mRNAs are abundant in the plate and well-watered root systems, enhanced by waterlogging, but depleted in the field, by WD and more so by SUB. Transcripts overrepresented in *pRSS1* in other patterns (16,17,19) encode proteins of cytosolic ribosomes (padj E−159), nucleoside metabolism (padj E−16), and cell wall biosynthesis (padj E−9), respectively, required for further proliferation or differentiation. We find that the environment has a pronounced effect on these mRNAs, particularly those in pattern 20.

To evaluate the environmental impact on the synthesis (S)-phase of the cell cycle, we examined the incorporation of fluorescence-labeled thymidine analog 5-ethynyl-2′ deoxyuridine (Click-iT EdU) (Kotogány et al., 2010) into a newly replicated DNA. Root tips of water-deprived seedlings do not show a significant change in fluorescence levels compared with the control (Figures 2B and S3C); however, these roots increase in length (Figure S6D). This may be through elongation growth that is accentuated by development of aerenchyma in rice (Niones et al., 2013; Watanabe et al., 2020). By contrast, the EdU signal was undetectable after SUB and largely restored within 24 h of desubmergence (Figures 2B and S3C), consistent with translational dynamics of mRNAs associated with DNA synthesis. This restriction of the S-phase by SUB is concomitant with significant reductions in primary root length of seedlings (Figure S3E), root biomass in older plants (Figure S1E), and maximum root length in the field (Singh et al., 2014).

To infer *cis*-regulation by TFs that may control the environmental responsiveness of DNA replication and cell-cycle genes, we surveyed THSs located nearby the 177 differentially expressed transcripts involved in these processes for enriched *cis*-regulatory motifs (Figure S4C; Table S6). Most of these transcripts are enriched in *pRSS1:TRAP* but show a dynamic signature in the *p35S:INTACT*-ATAC data, which includes proliferating cells (Figure S3B). The regulatory regions of these genes are significantly enriched for TFBSs of known regulators of cell proliferation. These include components of the conserved DREAM complex (dimerization partner, RB-like E2F and MuvB complex; E2F, DP, MYB3R) (Magyar et al., 2016; Sadasivam and DeCaprio, 2013; Shimotohno et al., 2021) and cell growth (GRF, TCP, and ERF) (Table S6). A WRKY TFBS, predicted to be bound by SUB-induced WRKY116, was also enriched in the THSs of these genes. Next, we generated a network of genes (small circles) and nodes of enriched TFBSs (large circles), where connections (edges) indicate if a target gene contains one or more of the TFBS in the THS (Figure S4C; Table S6). By coloring the nodes based on the change in the *pRSS1* translatome following SUB, the network highlights the conditional regulation of DNA synthesis and cell-cycle genes (Figure 2C).

To better understand the relationship between these TFBSs and gene activity, we evaluated the change in THS accessibility relative to the number of TFBSs they contain. Chromatin accessibility for THSs harboring the DP TFBSs show only a modest change under waterlogging, WD, or SUB ($p < 3E-4$; Figure 2D), suggesting that binding in those regions is less altered or there is insufficient resolution of accessibility dynamics. By contrast, numerous network genes possess one or more DEL-like TFBS within a THS. Their accessibility shows a positive correlation with the motif number present under WD ($p < 2E-16$) and a negative correlation under SUB ($p < 2E-16$). DELs are atypical E2Fs that function in division and growth control (Shimotohno et al., 2021; Sozzani et al., 2010a; Vlieghe et al., 2005). Monocot *DEL* duplicated independently from those of Arabidopsis (Figure S3F), and their roles are undefined. Based on our network, numerous SUB downregulated genes with the DEL TFBS function in DNA replication. These include minichromosome maintenance (MCM), origin of replication complex (ORC), and cell division cycle (CDC) components. Many of these genes are also inferred DP targets. Other downregulated DEL targets include the DREAM component *RBR1* and *TSO1-like*, which influence root meristem size in Arabidopsis (Wang et al., 2018). Notably, *DEL1/2* are present in the network as targets of TCP, ERF103, and WRKY116 (*DEL1* only). We postulate that a decline in DEL1 determines the conditional downregulation of the S-phase during SUB, due to the coincident decrease in *DEL1* mRNA, chromatin accessibility at DEL TFBSs, and DEL target gene transcripts (Figures 2C and 2E; Tables S5C and S6B). Another notable source node is the *MYB3R* TFBS that connects to G1/S transition and G2/M genes (i.e., *CYCB*s). These *MYB3Rs* are homologous to Arabidopsis *MYB3R1/4* that activate G2/M genes (Haga et al., 2011; Kobayashi et al., 2015) and At-MYB3R3/5 that repress the G2/M transition genes (Chen et al., 2017). In sum, this analysis connects seven-TF families with factors of DNA synthesis and division that are dynamically modulated in root tips by SUB.

Water availability treatments demonstrate reversible dynamics and stable identity of root cell population translatomes

To explore conditional responses of more specific meristematic and differentiated cells of the radial layers of roots, our study included TRAP lines that mark the meristematic endodermis (*pAtSCR*), meristematic cortex (*pCMZ*), lateral root primordia plus differentiated endodermis (*pCASP3*), exodermis and endodermis (*pLSI1*), and the quiescent center and developing xylem (*pQHB*) (Figures 3A, S2, and S4; Tables S1A and S1B). Multidimensional scaling and dominant pattern analysis illustrate reproducibility between biological replicates, conditional responses to waterlogging and WD, and signatures of promoter-defined translatomes (Figure S4A). The pronounced common effect of WD on each promoters' translatome contrasts with the modest impact of waterlogging, which was used to explore the similarities and differences of the *pCMZ*, *pAtSCR*, and *pCASP3* translatomes (Figure S4B), which profile meristematic ground tissue. Pattern 27 is uniquely enriched in these translatomes (Figure 3B) and contains a suite of auxin-related process genes from biosynthesis to response regulation (e.g., YUCCA family member *COW1*, auxin F-box binding proteins, and transcriptional regulators IAA14, AUXIN RESPONSE FACTOR [ARF]8/6B, respectively).

Next, by assessing TFBS enrichment in THSs nearby genes in the patterns, we find pattern 27 is enriched in E2F, DP, LBD, ERF, APETALA2 (AP2), and SQUAMOSA BINDING PROTEIN (SBP) motifs (Figure S4B; Table S6), whose cognate TFs possess roles in the cell cycle and root development. We created a network connecting the TFBSs inside THSs (source nodes) that are located near genes (target nodes) in this pattern (Figure 3C). This network includes genes important in splicing and small RNA-mediated regulation (*ARGONAUTE* (*AGO*) *1B/11/13/16*

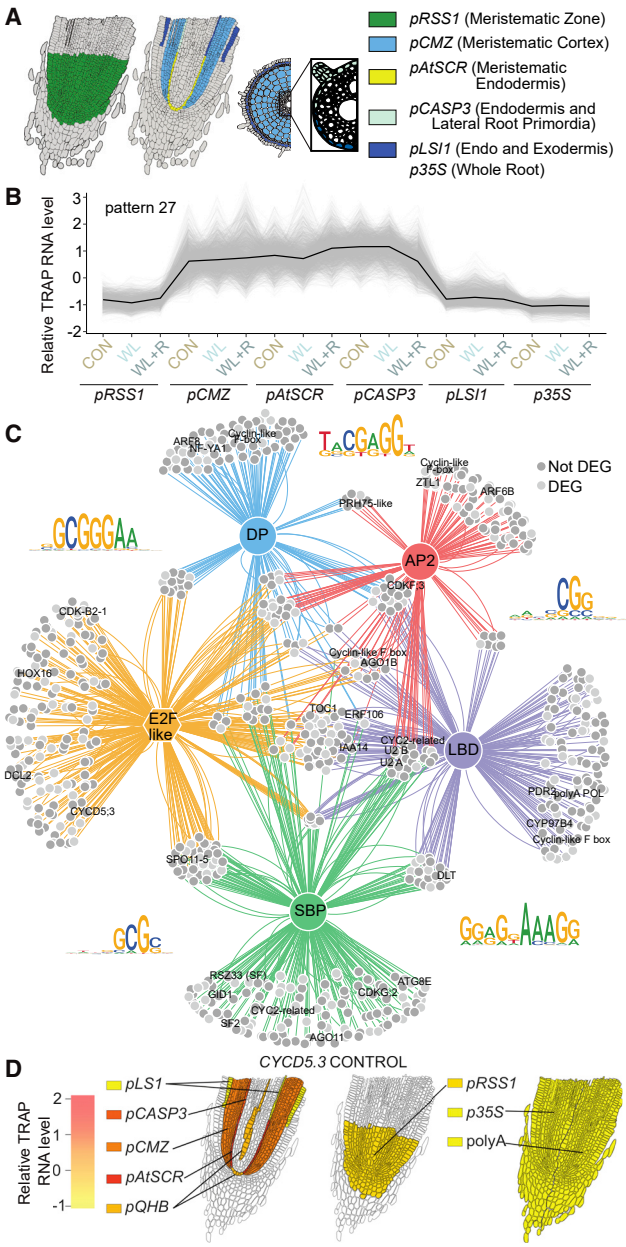

Figure 3. Translatomes of root domains in waterlogging and recovery conditions reveal a network enriched in ground tissue

(A) Polysomal mRNAs were obtained for different root domains marked in dividing cells (*pRSS1*), meristematic cortex (*pCMZ*) and endodermis (*pAtSCR*), differentiated endodermis (*pCASP3*), and exodermis (*pLSI1*) and other domains in *p35S*.

(B) A set of genes from a dominant pattern analysis showing enrichment in ground tissue translatomes (pattern 27).

(C) Inferred regulatory network of genes in pattern 27 active in ground tissue domains. Hexagons indicate TFBSs enriched in proximal THSs; big circles are TFBSs associated with TF genes in pattern 27. Target nodes are colored dark gray if they are not significantly differentially expressed in any of one or more comparisons (CON versus WD, CON versus WD+R, WD+R versus WD, CON versus WL, CON versus WL+R, or WL+R versus WL).

(D) Scaled transcript per million (TPM) reads displayed in a spatial heatmap for *CYCLIN D5;3* in pattern 27.

and *DICER-LIKE* (*DCL*) *2A/B*). miRNAs regulating ground tissue development can be cell autonomous or off-loaded from the phloem (non-cell autonomous); these target the TF source nodes AP2 and SBPs (Shao et al., 2019), as well as *ARF*-, *NF-Y*-, *AGO1B*-, and *TIR1*-like target nodes in the network (Table S4). The presence of clock regulatory genes *GIGANTEA* (*GI*), *ZEITLUPE-1* (*ZTL1*), and *TIMING OF CAB EXPRESSION* (*TOC1*) may relate to the clock's role in auxin signaling (Covington and Harmer, 2007) and lateral root development (Xuan et al., 2020). We also detect G1-/S-phase-specific cyclin D transcripts elevated in ground tissue translatomes, namely *CYCD5;3* (pattern 27) (Figure 3D) and *CYCD5;2* (pattern 29; Figure S4B) (Peres et al., 2007). In Arabidopsis, *AtCYCD6;1* determines early patterning of the cortex-endodermis initials (Sozzani et al., 2010b) and middle cortex (Bertolotti et al., 2021). It remains to be investigated if these cyclins function in key developmental cell divisions in rice.

Finally, we investigated how this network is altered by the environment. Notably, of the 2,077 genes in pattern 27, 69% are never significantly differentially expressed in these three cell populations in WD, waterlogging, or recovery conditions. The stable genes include most or all of the genes from the functional groups mentioned: auxin-regulated (*COW1*, *IAA14*, and *ARF6B*), small RNA-related (*AGO1B/13/16*, *DCL2A*), clock, and *CYCD5;3*. Overall, we identify a network that is enriched in meristematic ground tissue that is minimally perturbed by environmental conditions.

Water-deficit translatomes highlight core physiological responses and exodermal plasticity in suberin synthesis

Using the same analysis pipeline as before, we found that WD invokes a broad ABA transcriptional response (pattern 21, padj E−7) and distinct cell population-specific responses (Figures 4A and 4B; Table S5G). The promoters of pattern 21 genes are conditionally accessible and enriched for bZIP TFBSs (Table S6). These include the ABA response element (ABRE) bound by bZIP TFs that activate ABA responsive genes (Choi et al., 2000; Guiltinan et al., 1990). A pronounced upregulated pattern specific to *pLSI1*-marked cells (pattern 20) is enriched for genes involved in suberin biosynthesis (padj E−3). We used Fluorol Yellow (FY) staining to confirm increased suberin deposition primarily in the exodermal cell layer under WD, whereas the endodermis is suberized independent of condition (Figures 4C and S1G). Next, we implemented a coexpression network approach (Data S2; Wisecaver et al., 2017) using all transcriptome and translatome data to define small (<10 gene) to large (100+) modules (Data S2) that represent activity of specific pathways in one or more cell populations (Table S7). A 203 gene module in cells marked by *pLSI1* (N5:MOD000731; Table S7) defines a WD-responsive suberin barrier, encompassing the complete biosynthetic pathway for suberin as currently understood, from monomer synthesis to transport and polymerization (Vishwanath et al., 2015; Data S2; Figure S5A). The genes include the suberin transporter *ABCG5* (Shiono et al., 2014) and enzymes whose functional roles have been validated for homologous proteins in other species such as aliphatic suberin feruloyl transferase (ASFT) (Gou et al., 2009; Molina et al., 2009) and GDSL esterase/lipases (Lashbrooke et al., 2016; Ursache et al., 2021;

CellPress
OPEN ACCESS

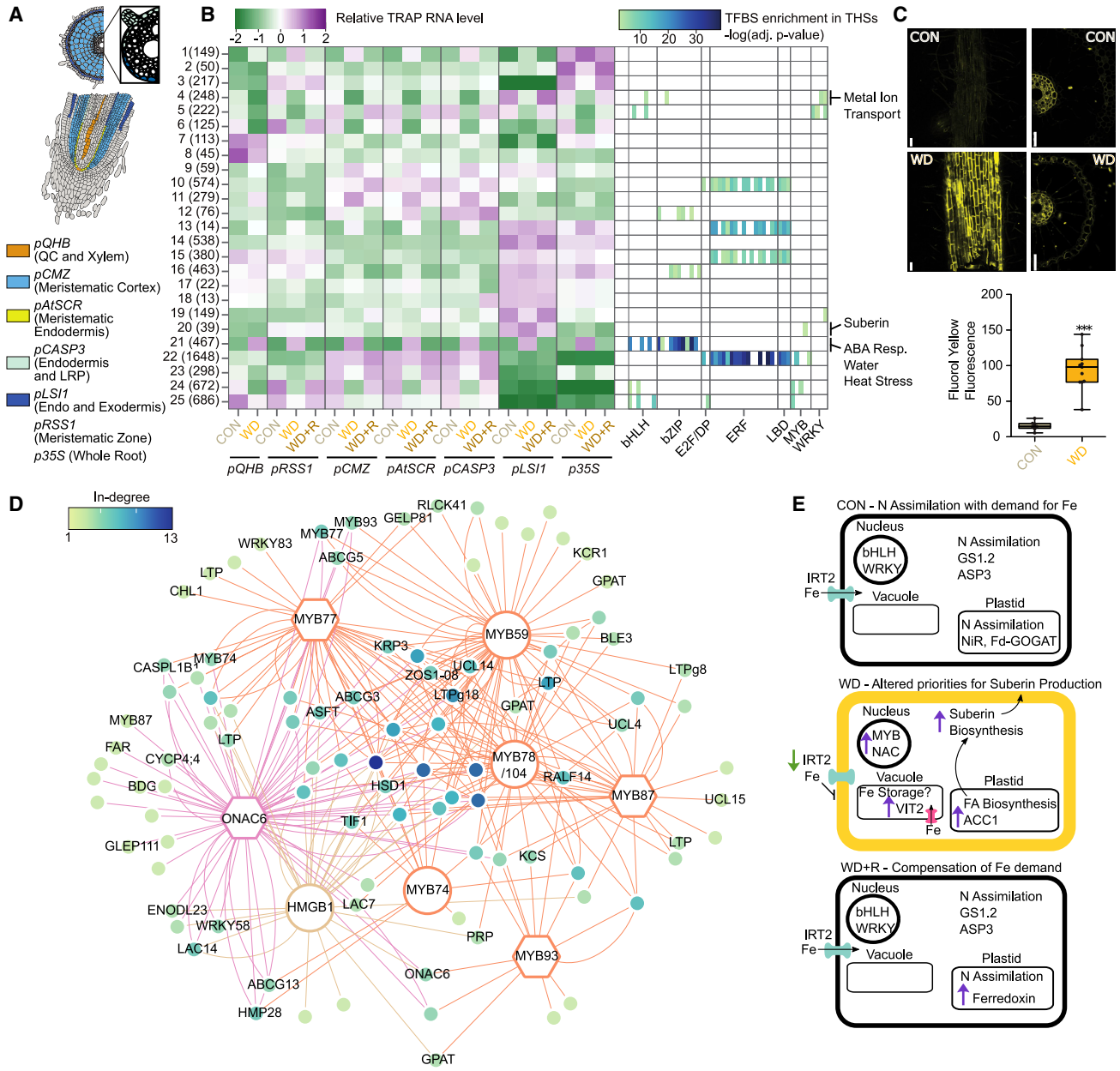

Figure 4. Responses to water deficit and recovery across root domains reveal dynamic patterns of translatomes and contrasting metabolic pathways

(A and B) Gene activities of cell populations of meristematic regions including dividing cells (*pRSS1*), quiescent center and metaxylem (*pQHB*), cortex (*pCMZ*), and endodermis (*pAtSCR*) were contrasted with differentiated regions in endodermis (*pCASP3*), endodermis/exodermis (*pLSI1*), and others included in *p35S*. A heatmap depicts scaled TPM TRAP RNA levels for genes with differences in control, water deficit, and 1-day recovery calculated by dominant pattern analysis and enrichment of TF binding sites in THSs located nearby genes in each pattern. Each bar represents enrichment for a TFBS within a specific TF family. Number of genes in pattern in parenthesis.

(C) Fluorol Yellow (FY) staining of rice crown roots for suberin in longitudinal views of the exodermis and radial cross sections. Quantification of exodermal FY signal of control and WD plants by corrected total cell fluorescence (CTCF). Asterisks indicate significant differences by Student's t test ($p = 0.005$).

(D) An inferred regulatory network of genes in coexpression module N5:MOD000731 enriched for genes associated with suberin biosynthesis and the *pLS1* cell population under water deficit. Large circles indicate TFBSs enriched in proximal THSs; hexagons are TFBSs associated with TF genes in the coexpression module; colors indicate TF family; in-degree reflects the number of TFBSs connected to a given gene.

(E) A model of dynamics within the *pLSI1*-marked cells. Briefly, transcripts associated with N assimilation processes and Fe uptake are translated in control conditions. In the water-deficit translatome, Fe uptake is downregulated and plastidial fatty acid biosynthesis is upregulated, feeding into suberin biosynthesis and the deposition of apoplastic suberin. In the recovery condition, the Fe uptake translatome signature is restored, and there is further upregulation of N assimilation genes, including the ferredoxin cofactor that uses Fe in N assimilation.

Figure S5A). This coexpression module enabled construction of a WD-promoted suberin network of regulation dominated by MYB and NAC TFs (Figure 4D). One of the MYB TFBSs (M07061) originates from the suberin-regulating *At*MYB107 (Lashbrooke et al., 2016).

Although waterlogging increases exodermal suberization (Figure S1G), especially toward the tip of rice roots (Shiono et al., 2014), we did not observe upregulation of the suberin module in the *pLSI1* WL translatome obtained after 5 days or waterlogging. Suberin biosynthesis may occur rapidly in WL roots or could be more prolonged under WD due to the increased surface area of exodermal cells of elongating roots.

Suberin is a complex polymer that likely burdens the synthesizing cells with new metabolic demands, including an increased need for fatty acid biosynthesis by the plastid. Additionally, this barrier may require alterations in the apoplast and active transport pathways. Other dominant patterns (4, 14, 19) of *pLSI1*-marked cells show pronounced downregulation under WD (Figure 4B; Table S5G). Of these, pattern 4 was enriched for transition metal ion transport (padj E−3) and included *IRT2*, encoding an iron (Fe) transporter that is upregulated upon Fe deficit (Ishimaru et al., 2006). *IRT2* is in the *pLSI1*-enriched but WD-reduced coexpression module N2:MOD000130 (Data S2), along with other genes that may play a role in Fe homeostasis. Histochemical visualization of Fe by use of Perls staining with DAB intensification marks the exodermis and epidermis and significantly diminishes across the whole root system following WD (Figure S1H). This is consistent with the detection of an Fe maxima in the outer layers of tomato roots by synchrotron micro X-ray fluorescence microscopy (Terzano et al., 2013). The Fe deficiency-response bHLH TFs IRO2, IRO3, and PRI1 (Ogo et al., 2006; Wang et al., 2020; Zhang et al., 2017) are also enriched in *pLSI1* translatomes but downregulated by WD as shown using a spatialHeatmap (Figure S5B). Consistently, pattern 4 genes show enrichment for bHLH and WRKY TFBSs (Figure 4B), including members that are WD reduced (Figure S5B). *IRO2* is exodermal but not endodermal expressed in rice (Ogo et al., 2011), supporting the conclusion that Fe demand or uptake by the exodermis is reduced by WD.

Metals including Fe are cofactors for reductive biochemical reactions, leading us to consider processes that may be altered to reduce Fe demand in *pLSI1*-marked cells under WD. Nitrogen (N) assimilation is an Fe-dependent process requiring the plastidal enzymes GOGAT, nitrite reductase (NiR), and the Fe-requiring ferredoxin cofactor; these mRNAs are highly abundant in *pLSI1* translatomes. Indeed, NiR (*PSR1*) is in a coexpression module that includes the N assimilation-related gene *ASN1* (encoding asparagine synthetase) and a ferredoxin (*FDVI*) (N3:MOD001584, Data S2). Transcripts in this *pLSI1*-enriched module peak during WD recovery. A translatome signature for N regulation is also enriched in the exodermis of tomato (Kajala et al., 2021). We propose a model (Figure 4E), wherein under control conditions, the *pLSI1*-marked cells uptake Fe via IRT2, at least in part for incorporation into ferredoxin. Under WD, elevated suberin biosynthesis requires more plastidal fatty acid biosynthesis by *ACETYL-COA CARBOXYLASE 1* (*ACC1*), which may be favored over N assimilation, leading to reduced Fe demand along with elevation of a vacuolar Fe transporter (*VIT2*) (Figure S5B) to sequester excess Fe. As observed for the metal ion module, the shift in N metabolism in the *pLSI1* cell population appears to be reversible. Upon rewatering, the rise in translated N assimilation module mRNAs indicates reprioritization of N and Fe uptake. These dynamics could reflect an inability of exodermal plastids to conduct suberin biosynthesis and N assimilation simultaneously or changes in cellular capacity to uptake Fe or N after additional suberization, or a combination of the two. WD concomitantly limits N availability since ammonia and nitrates are water soluble, and there is a trade-off between N metabolism and WD tolerance (Araus et al., 2020). We hypothesize that shifting activities of bHLHs and WRKYs to MYBs and NACs in the exodermis modulates dynamics in suberin, Fe and N uptake, and transport to water availability.

Hierarchical regulation of gene expression in cell populations and conditions

To infer which TFs might play key upstream regulatory roles versus those that act downstream in transcriptional regulatory cascades, we profiled accessible chromatin in *p35S*, *pQHB*, and *pCMZ*-marked nuclei, which in all cases yielded reads primarily in genic and promoter regions (Figures 5A, 5B, and S2; Table S8). Using 16 sets of paired chromatin accessibility and translatome data, we implemented the Taiji pipeline for gene regulatory network inference (Zhang et al., 2019a; Figure 5C). Briefly, we mapped TFBSs associated with 741 rice TF genes in the CisBP Database (Lambert et al., 2019; Weirauch et al., 2014) to THSs. This predicted a genome-wide binding network for each dataset that connected TFs to target genes. Next, all genes were weighted based on relative transcript abundance in the corresponding translatome data. Finally, the PageRank algorithm was used to reallocate weight to recognize putative driver TFs that are more frequently regulating genes, including genes encoding other TFs. This identified 136 TFs with conditional and cell population relevance by clustering PageRank scores across all networks (Figure 5D; Table S8). The *p35S* data highlight conditional TF hierarchies for WD, SUB, and the field (clusters 8, 9, and 10). Consistent with their role as direct first responders to ABA signaling (Choi et al., 2000), ABRE-binding factors are predicted as drivers of other TFs including *HOX22* (Zhang et al., 2012). Driver TFs recognized in the population of cells marked by *pQHB*, the quiescent center, and developing xylem (Figures 5D and 5F; clusters 4–6) varied by condition. In well-watered roots, these include *QHB* itself, as well as conserved regulators of xylem development including four HD-ZIPIIIs, called HBs in rice (2 PHB/PHV-like and 2 REV-like, phylogenetically resolved in Kajala et al., 2021), and three VND-like NACs, called secondary wall NACs (SWNs) (Figure 5F). The TF with the highest PageRank score in control conditions is the bHLH TMO5 LIKE 1 (TMO5L1) with orthology to *AtTMO5*, a key regulator of vascular development (Schlereth et al., 2010) that is uncharacterized in rice. HD-ZIPIIIs are predominant in the control condition-specific cluster 4 (Figure 5D), with downregulation under WD consistent with observations for Arabidopsis (Bloch et al., 2019). The condition-stable *pQHB* cluster includes the TMO5-like and VND-like NACs. A TF of note in *pCMZ*-marked cells under waterlogging is *RICE STARCH REGULATOR 1* (*RSR1*), limits starch biosynthesis (Fu and Xue, 2010), and is predicted to bind the AP2 TFBS enriched in the ground tissue network (Figure 3C). This unsupervised analysis resolves known

CellPress
OPEN ACCESS

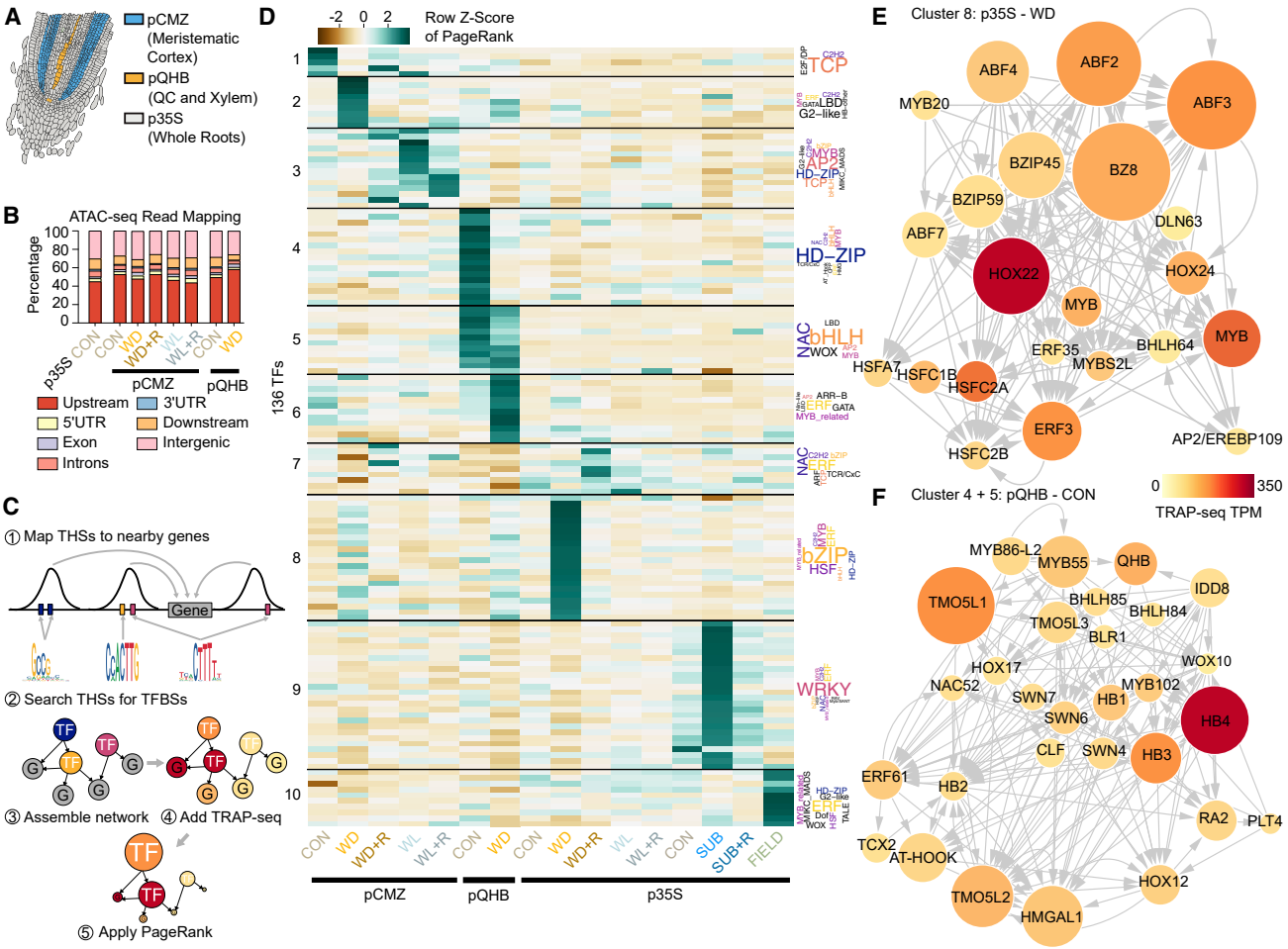

Figure 5. Gene regulatory network modeling predicts driver TFs involved in cell population and condition-regulated gene expression

(A) Cell populations assayed with ATAC-seq and TRAP-seq; *pCMZ*, *pQHB*, and *p35S*.

(B) Reads from cell population-specific ATAC-seq map to expected regions of the genome, similar to data for *p35S* (Figure S2A).

(C) An overview of the Taiji analysis pipeline used to identify driver TFs. For each cell population and condition, THSs are associated with proximal genes and searched for TFBSs, a putative binding network is built, TRAP-seq data are overlaid and the PageRank algorithm prioritizes driver TFs.

(D) Heatmap of PageRank values across the network for genes with specific activity (Row Z > 2.5 in at least one condition or cell population). TF Families in each cluster are summarized with a word cloud.

(E and F) Predicted regulatory network for specific clusters where node size scales with PageRank score and color with TRAP-seq TPM. Arrows indicate predicted regulatory interactions. (E) Transcription factors from clusters 4 and 5, with data from *pQHB* under CON. (F) Transcription factors from cluster 8, with data from *p35S* under WD.

conditional hierarchies and conserved developmental regulators (i.e., xylem), which both validate the approach and yield new targets for trait manipulation.

Cell population identity from plate to field

To characterize the identity of cell-type translatomes in an agricultural context, we grew eight TRAP lines (Figure 6A) in a paddy field and evaluated their translatomes (Figures 6B and S6B). These included lines using *pHMA5* (pericycle) (Deng et al., 2013), *pNRAMP3* (phloem companion) (Yang et al., 2013), *pSHR1* (stele) (Cui et al., 2007), and *pEXPB5* (Won et al., 2010). The expression patterns of these promoter-gene constructs agree with previous reports, except *pEXPB5*, that marks epidermal cells in the elongation zone in our system, rather than hair cells as reported (Data S1). The translatomes of field-grown roots were evaluated by ROKU (Kadota et al., 2006), identifying 15,402 cell population-enriched genes (CPEGs) (Figure 6C; Table S9) and uncovering new and evolutionarily conserved markers (Figure 6D), for example, 67 *pNRAMP3* CPEGs in the same gene family as a core Arabidopsis phloem companion cell genes (Mustroph et al., 2009a; Table S9).

Marker genes whose promoters drive the TRAP constructs show corresponding transcript enrichment with two exceptions (Figure S6C). Notably, *SHR1* mRNA is enriched in the *pLSI1* translatome (Figure S6C), although both *in situ* detected mRNA (Cui et al., 2007) and *pSHR1:TRAP/GUS* expressions were limited to the stele (Data S1). Regulatory elements outside the promoter region used (Figure S6D) could promote endodermal transcription or the mRNA could move outward. Also, phase separation could possibly control referential translation in the endodermis (Zhang

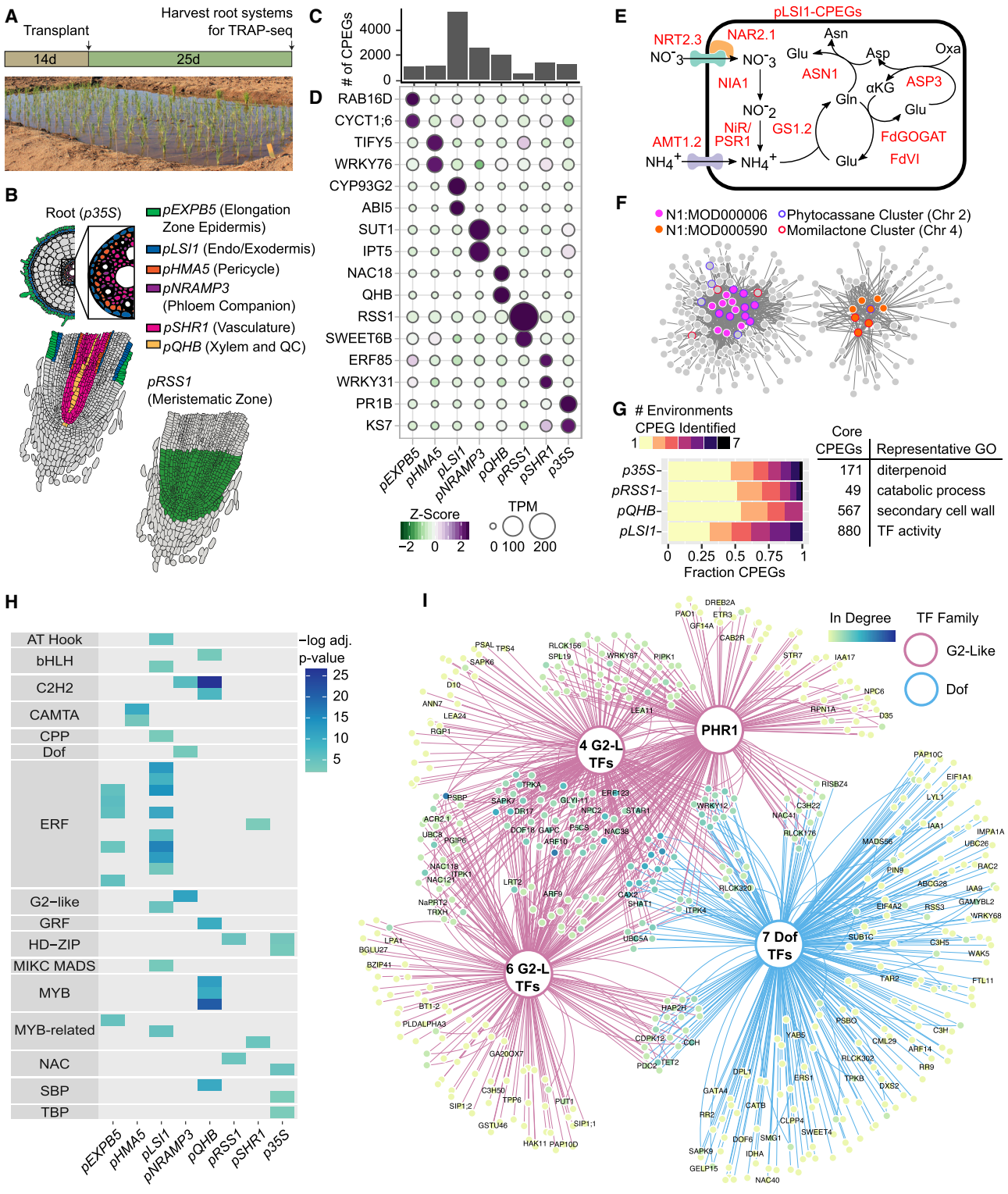

Figure 6. A field-grown translatome atlas reveals domain partitioning of metabolism and regulation

(A) Overview of experimental design TRAP-seq was conducted on whole root systems of rice plants grown in a paddy field.

(B) Promoter-defined cell populations profiled.

(C) Number of CPEGs identified for each cell population.

(D) Strongly enriched CPEGs identified as markers of each cell population.

(legend continued on next page)

et al., 2019b). Unlike in Arabidopsis, maize SHR1 protein moves outward beyond the endodermis to cortical cells (Ortiz-Ramírez et al., 2021). There may be more variation and innovation in *SHR* function than previously considered (Cui et al., 2007).

The greatest number of CPEGs were recognized for *pLSI1* (Figure 6C). These include an N assimilation-related coexpression module (Data S2; Table S9), the complete pathway from ammonia and nitrate import to asparagine biosynthesis (Figure 6E; Table S9), and significant overlap with the conserved rice-Arabidopsis N regulatory network (Obertello et al., 2015) (odds ratio 2.4, p = 4.29E−7) (Table S9). Although *pLSI1* is active in the differentiated endodermis and exodermis, we predict N metabolism is predominantly exodermal, given that NiR, GOGAT, and ammonium transporters are enriched in the rice exodermis (Hayakawa et al., 1999; Konishi and Ma, 2021) and a N transcriptional network is enriched in the tomato exodermis (Kajala et al., 2021).

As the paddy field is a multifactorial environment, we considered the possibility of signatures of specialized metabolism associated with microbial interactions. The coexpression module analysis identified two connected diterpene biosynthetic gene clusters on chromosomes 4 and 2 that produce momilactones (Shimura et al., 2007) and phytocassanes (Swaminathan et al., 2009), respectively, with enrichment in *p35S*-marked cells (Figure 6F; Data S2). These diterpenes have roles in microbial and allelopathic interactions (Schmelz et al., 2014). In paddy roots, the phytocassane but not the momilactone module is upregulated (Data S2). The higher activity of the phytocassane module in field-grown but not in pot-grown plants may reflect distinctions in microbial interactions.

Next, we sought to evaluate the robustness of cell population translatomes across developmental age and environmental conditions, which can reveal key regulators and processes central to cell types and tissues (Iyer-Pascuzzi et al., 2011). To identify genes consistently enriched in cell populations across conditions (core CPEGs), ROKU was applied to determine CPEGs independently in each environment (plate, greenhouse conditions, and field) for cell populations surveyed (Figure 6G). We find that *pRSS1* core CPEGs are enriched for catabolic processes, consistent with the energy-demanding process of growth and cell division in this cell population. *pQHB* core CPEGs are enriched for secondary cell wall-related GO terms, indicating that the construction of a secondary cell wall is central to xylem cell identity, regardless of condition or age. *pLSI1* core CPEGs showed GO enrichment for DNA-binding TF activity, illustrating that stably enriched genes can have regulatory function. These TFs include eight GRAS family members, among which are *SCR1/2* and *SHR1*. Of the 14 TFs that mark mature exodermal cells by scRNA-seq (Zhang et al., 2021), only WRKY107 was a core CPEG for *pLSI1*. Two TFs (ZFP182 and WRKY24) enriched by scRNA-seq in exodermal cells are SUB response drivers in our study (Figure 5D). These may reflect transcriptome versus translatome differences or effects of the environment or protoplasting.

Finally, we defined putative regulatory networks of cell populations. To do so, we tested for enrichment of known TFBSs in THSs proximal to each set of CPEGs (Figure 6H; Table S6). Among *pNRAMP3* CPEGs, we identified TFs that may bind these *cis*-elements and assembled a target gene network (Figure 6I). These include orthologs of Arabidopsis G2-like and Dof TFs that have roles in phloem development (*APL* [Bonke et al., 2003]; *PEARs* [Miyashima et al., 2019]). One predicted regulatory interaction is between Dof TFs and *FTL11*, a homolog of Arabidopsis *FT* that is known to be regulated by cycling DOF factors (CDFs) in phloem companion cells of Arabidopsis to control flowering (Goralogia et al., 2017).

DISCUSSION

Here, we provide an atlas of the dynamic and reversible environmental reprograming in response to water extremes at the epigenetic and transcript levels in root cell populations. We establish computational pipelines that integrate chromatin and translatome data to define gene *cis*-regulatory networks and recognize key TFs governing responses to a dynamic environment. The study identifies reversible epigenetic and transcriptomic plasticity as a hallmark of responses to water extremes. Stable signatures include genes essential for cell division and differentiation of cell types. Dynamic signatures include core stress responses to SUB and WD. By contrast, waterlogging minimally impacts the epigenome and translatome of rice roots.

The evaluation of proliferating cells in the root tips determines that SUB limits DNA synthesis, concomitant with modulated accessibility at E2F-like DEL TFBSs of genes associated with DNA replication and G1/S and G2/M progression. The observation of differential accessibility associated with TFBSs suggests that some TFs promote the accessibility of chromatin (i.e., DELs in the cell-cycle network). Association of TFBSs and chromatin accessibility in animal systems (Blatti et al., 2015) recovered known "pioneer factors" that bind inaccessible nucleosomal DNA and promoted accessibility (Zaret and Carroll, 2011). These factors are usually defined in the context of permanent developmental transitions. For example, Arabidopsis LEAFY reprograms cells for flowering (Jin et al., 2021; Lai et al., 2021). It remains to be seen if pioneer-like factors act transiently in stress responses to facilitate dynamic opening or closing of chromatin regions.

Assaying translatomes of roots in five irrigation scenarios uncovers that meristematic ground tissue maintains a transcript

(E) A pathway for N assimilation from transport of ammonia or nitrate to asparagine, the main form of mobile N in the plant. Gene names in red are *pLSI1* CPEGs and form a complete pathway. αKG, alpha-ketoglutarate; Oxa, Oxaloacetate.
(F) Coexpression modules that contain momilactone (Chr 4) and phytocassane (Chr 2) gene clusters. Shown are the two modules and first-neighbors of module members. Edge thickness corresponds with edge weights in the coexpression network. Sixteen of 24 of these genes are *p35S* CPEGs.
(G) Fractions of CPEGs identified in multiple environmental conditions (Figure 1A) profiled for four cell populations and representative GO terms for the most highly conserved (core) CPEGs across environments. The maximum number of environments varies by promoter; 7 for p35S and pRSS1; 6 for pLSI1; and 4 for pQHB.
(H) Enrichment of TFBSs present in THSs proximal to CPEGs across cell populations. Each bar represents enrichment for a TFBS within a specific TF family.
(I) A motif network for translated mRNAs enriched in *pNRAMP3* and TFBSs present in the promoters. In-degree reflects the number (1 to 13) of TFBSs connected to a given gene.

signature characterized by auxin regulation, small RNA regulation, and the circadian clock. The barrier cell layers of the endo- and exo-dermis, however, appear plastic in response to WD. These upregulate suberin biosynthesis and downregulate Fe ion transport. Upon rewatering, certain N assimilation genes transcripts are upregulated in the translatome. Barrier cells also show enrichment of a N assimilation pathway in the paddy field. Roots of droughted sorghum also downregulate mRNAs associated with Fe uptake (Xu et al., 2018). In Arabidopsis, Fe deficiency causes a delay in suberization of the endodermis (Barberon et al., 2016) and mutations that increase endodermal suberin accumulate less Fe in shoots (Hosmani et al., 2013; Kamiya et al., 2015), indicating a trade-off between Fe uptake and suberization. There may be additional complexity in the rice exodermis, where we hypothesize N assimilation requires Fe. Tools to investigate cell-type-specific ionomes, proteomes, and metabolomes (Plant Cell Atlas Consortium et al., 2021) could help to validate this hypothesis and enable optimal engineering of stress-resilient barrier cells.

The integration of chromatin and translatome data of cell populations to recognize and rank TFs regulating environmental response and development confirms that regulators of WD responses and xylem development are conserved across species. The ability to predict top candidates for manipulating growth and development in response to the environment can guide functional validation and engineering strategies. Finally, the atlas of root translatomes from cell populations of field-grown rice provides a reference for spatial gene activity in an agronomically relevant multifactorial environment. We also use this condition and the others surveyed to recognize sets of genes that are stably enriched in cell populations across environments, furthering the definition of cell-type domains, identifying candidate markers for use across environments.

We anticipate use of this resource for studying the molecular architecture of environmental responses will complement single-cell sequencing techniques, which can resolve developmental trajectories of mRNAs and chromatin accessibility (Shahan et al., 2021), as they become amenable for evaluation of dynamic responses (Wang et al., 2021). It may be valuable to intersect our findings with nucleotide variants in resequenced rice accessions that show evidence of selection in relation to adaptive traits associated with resilience to intermittent WD (Groen et al., 2020, 2022). This resource opens new avenues for breeding and engineering climate-resilient crops by enhancement of plant responses to the environment through manipulation of gene regulatory circuitry.

Limitations of the study

Our promoter-driven approaches and discrete states as opposed to time course profiling mean that the spatiotemporal regulation of gene activity has not been fully explored. The cell types marked may have earlier or heterogeneous responses across the root system that we were not able to detect, and the cell-type compositions of root types may themselves change under stress. In our network modeling, the CisBP database includes TFBSs for about half of rice TFs. New cistrome-scale DAP-seq and ChIP-seq studies of rice TFs will likely increase the accuracy from TFBS mapping in accessible chromatin regions from our data. Currently, we are unable to determine if TF binding to target genes is activating, repressing, or inconsequential. The predicted regulatory modules could include both activators and repressors working antagonistically to maintain transcriptional homeostasis. We have not specifically sought to predict repressors in our data, since not enough is known about the relationship between repressors and accessible chromatin.

STAR★METHODS

Detailed methods are provided in the online version of this paper and include the following:

- KEY RESOURCES TABLE
- RESOURCE AVAILABILITY
  - Lead contact
  - Materials availability
  - Data and code availability
- EXPERIMENTAL MODEL AND SUBJECT DETAILS
  - Rice genetic material
  - Rice growth conditions and stress treatments
- METHOD DETAILS
  - INTACT and ATAC-seq
  - TRAP and RNA-seq libraries
  - EdU staining and growth measurements
  - Suberin staining
  - Perls-DAB staining
- QUANTIFICATION AND STATISTICAL ANALYSIS
  - ATAC-seq and RNA-seq data processing
  - RNA-seq differential expression, mapping of chromatin accessibility, identification of Transposase Hypersensitive Sites, and evaluation of accessibility changes between conditions
  - Network construction
  - Identification of Cell Population Enriched Genes (CPEGs)
  - Phylogeny

SUPPLEMENTAL INFORMATION

Supplemental information can be found online at https://doi.org/10.1016/j.devcel.2022.04.013.

ACKNOWLEDGMENTS

We thank A. Kettenburg, S. Winte, R. Mataki, M. Natividad, K. Tran, K. Oda, J. Carale, M. Guillemin, S. Su, and M. Yamamoto for experimental assistance; K. Kajala, S. Gray, J. Rodriguez, M. Bajic, D. West, G.A. Mason, D. Kosma, Z. Wahrenburg, and Bailey-Serres and Nagel Lab members for discussions; A. Canto-Pastor and L. Shaar-Moshe for discussions and manuscript critique. Funding support for this work: NSF PGRP grants IOS-1238243 and 1856749 to R.B.D., N.R.S., S.M.B., and J.B.-S.; NSF PGRP IOS-1810468 to T.G. and J.B.-S.; NSF DGE-1922642 to A.T.B. and J.B.-S.; and USDA NIFA 1026477 to A.T.B; ANPCyT PICT 2018-00503 and PICT 2019-01970 to M.A.R.

AUTHOR CONTRIBUTIONS

Conceptualization, M.A.R., A.T.B., G.C.P., J.B.-S., T.G., E.Y., S.M.B., N.R.S., and R.B.D.; data curation, M.A.R., A.T.B., G.C.P., and J.B.-S.; formal analysis, M.A.R., A.T.B., G.C.P., J.B.-S., E.Y., and G.Z.A.; funding acquisition, J.B.-S., T.G., S.M.B., N.R.S., R.B.D., and A.T.B.; investigation, M.A.R., A.T.B., G.C.P., J.B.-S., E.Y., C.D., S.C., M.J.P., E.F., and J.V.; methodology, M.A.R., A.T.B.,

G.C.P., and J.B.-S.; project administration, J.B.-S.; software: M.A.R., A.T.B., T.G., and J.Z.; supervision, M.A.R., G.C.P., J.B.-S., and T.G.; visualization, M.A.R., A.T.B., J.B.-S., T.G., and J.Z.; writing – original draft, M.A.R., A.T.B., and J.B.-S.; writing – reviewing & editing, M.A.R., A.T.B., G.C.P., J.B.-S., T.G., E.Y., G.Z.A., S.M.B., N.R.S., and R.B.D.

DECLARATION OF INTERESTS

The authors declare no competing interests.

INCLUSION AND DIVERSITY

One or more of the authors of this paper self-identifies as an underrepresented ethnic minority in science. One or more of the authors of this paper received support from a program designed to increase minority representation in science. The author list of this paper includes contributors from the location where the research was conducted who participated in the data collection, design, analysis, and/or interpretation of the work.

Received: August 16, 2021
Revised: February 10, 2022
Accepted: April 7, 2022
Published: May 2, 2022

REFERENCES

Akmakjian, G.Z., and Bailey-Serres, J. (2022). Gene regulatory circuitry of plant-environment interactions: scaling from cells to the field. Curr. Opin. Plant Biol. *65*, 102122.

Araus, V., Swift, J., Alvarez, J.M., Henry, A., and Coruzzi, G.M. (2020). A balancing act: how plants integrate nitrogen and water signals. J. Exp. Bot. *71*, 4442–4451.

Barberon, M., Vermeer, J.E.M., De Bellis, D., Wang, P., Naseer, S., Andersen, T.G., Humbel, B.M., Nawrath, C., Takano, J., Salt, D.E., et al. (2016). Adaptation of root function by nutrient-induced plasticity of endodermal differentiation. Cell *164*, 447–459.

Bertolotti, G., Unterholzner, S.J., Scintu, D., Salvi, E., Svolacchia, N., Di Mambro, R., Ruta, V., Linhares Scaglia, F., Vittorioso, P., Sabatini, S., et al. (2021). A PHABULOSA-controlled genetic pathway regulates ground tissue patterning in the Arabidopsis root. Curr. Biol. *31*, 420–426.e6.

Blatti, C., Kazemian, M., Wolfe, S., Brodsky, M., and Sinha, S. (2015). Integrating motif, DNA accessibility and gene expression data to build regulatory maps in an organism. Nucleic Acids Res. *43*, 3998–4012.

Bloch, D., Puli, M.R., Mosquna, A., and Yalovsky, S. (2019). Abiotic stress modulates root patterning via ABA-regulated microRNA expression in the endodermis initials. Development *146*, dev177097.

Bonke, M., Thitamadee, S., Mähönen, A.P., Hauser, M.-T., and Helariutta, Y. (2003). APL regulates vascular tissue identity in Arabidopsis. Nature *426*, 181–186.

Brumbarova, T., and Ivanov, R. (2014). Perls staining for histochemical detection of iron in plant samples. Bio Protoc. *4*, e1245.

Buenrostro, J.D., Giresi, P.G., Zaba, L.C., Chang, H.Y., and Greenleaf, W.J. (2013). Transposition of native chromatin for fast and sensitive epigenomic profiling of open chromatin, DNA-binding proteins and nucleosome position. Nat. Methods *10*, 1213–1218.

Capella-Gutiérrez, S., Silla-Martínez, J.M., and Gabaldón, T. (2009). trimAl: a tool for automated alignment trimming in large-scale phylogenetic analyses. Bioinformatics *25*, 1972–1973.

Chen, P., Takatsuka, H., Takahashi, N., Kurata, R., Fukao, Y., Kobayashi, K., Ito, M., and Umeda, M. (2017). Arabidopsis R1R2R3-Myb proteins are essential for inhibiting cell division in response to DNA damage. Nat. Commun. *8*, 635.

Choi, H., Hong, J., Ha, J., Kang, J., and Kim, S.Y. (2000). ABFs, a family of ABA-responsive element binding factors. J. Biol. Chem. *275*, 1723–1730.

Clark, N.M., Buckner, E., Fisher, A.P., Nelson, E.C., Nguyen, T.T., Simmons, A.R., de Luis Balaguer, M.A., Butler-Smith, T., Sheldon, P.J., Bergmann, D.C., et al. (2019). Stem-cell-ubiquitous genes spatiotemporally coordinate division through regulation of stem-cell-specific gene networks. Nat. Commun. *10*, 5574.

Covington, M.F., and Harmer, S.L. (2007). The circadian clock regulates auxin signaling and responses in Arabidopsis. PLoS Biol. *5*, e222.

Cui, H., Levesque, M.P., Vernoux, T., Jung, J.W., Paquette, A.J., Gallagher, K.L., Wang, J.Y., Blilou, I., Scheres, B., and Benfey, P.N. (2007). An evolutionarily conserved mechanism delimiting SHR movement defines a single layer of endodermis in plants. Science *316*, 421–425.

Deal, R.B., and Henikoff, S. (2010). A simple method for gene expression and chromatin profiling of individual cell types within a tissue. Dev. Cell *18*, 1030–1040.

Deng, F., Yamaji, N., Xia, J., and Ma, J.F. (2013). A member of the heavy metal P-type ATPase OsHMA5 is involved in xylem loading of copper in rice. Plant Physiol. *163*, 1353–1362.

Dorrity, M.W., Alexandre, C.M., Hamm, M.O., Vigil, A.-L., Fields, S., Queitsch, C., and Cuperus, J.T. (2021). The regulatory landscape of *Arabidopsis thaliana* roots at single-cell resolution. Nat. Commun. *12*, 3334.

Fellows, I. (2012). wordcloud: word clouds. R package version 2: 109. https://cran.r-project.org/web/packages/wordcloud/wordcloud.pdf.

Finn, R.D., Clements, J., and Eddy, S.R. (2011). HMMER web server: interactive sequence similarity searching. Nucleic Acids Res. *39*, W29–W37.

Fu, F.-F., and Xue, H.-W. (2010). Coexpression analysis identifies Rice Starch Regulator1, a rice AP2/EREBP family transcription factor, as a novel rice starch biosynthesis regulator. Plant Physiol. *154*, 927–938.

Fukao, T., Yeung, E., and Bailey-Serres, J. (2011). The submergence tolerance regulator SUB1A mediates crosstalk between submergence and drought tolerance in rice. Plant Cell *23*, 412–427. https://doi.org/10.1105/tpc.110.080325.

Gasch, P., Fundinger, M., Müller, J.T., Lee, T., Bailey-Serres, J., and Mustroph, A. (2016). Redundant ERF-VII transcription factors bind to an evolutionarily conserved *cis*-motif to regulate hypoxia-responsive gene expression in Arabidopsis. Plant Cell *28*, 160–180.

Goralogia, G.S., Liu, T.-K., Zhao, L., Panipinto, P.M., Groover, E.D., Bains, Y.S., and Imaizumi, T. (2017). CyclinG dof FACTOR 1 represses transcription through the TOPLESS co-repressor to control photoperiodic flowering in Arabidopsis. Plant J. *92*, 244–262.

Gou, J.-Y., Yu, X.-H., and Liu, C.-J. (2009). A hydroxycinnamoyltransferase responsible for synthesizing suberin aromatics in Arabidopsis. Proc. Natl. Acad. Sci. USA *106*, 18855–18860.

Groen, S.C., Ćalić, I., Joly-Lopez, Z., Platts, A.E., Choi, J.Y., Natividad, M., Dorph, K., Mauck, W.M., 3rd, Bracken, B., Cabral, C.L.U., et al. (2020). The strength and pattern of natural selection on gene expression in rice. Nature *578*, 572–576.

Groen, S.C., Joly-Lopez, Z., Platts, A.E., Natividad, M., Fresquez, Z., Mauck, W.M., Quintana, M.R., Cabral, C.L.U., Torres, R.O., Satija, R., et al. (2022). Evolutionary systems biology reveals patterns of rice adaptation to drought-prone agro-ecosystems. Plant Cell *34*, 759–783.

Guiltinan, M.J., Marcotte, W.R., Jr., and Quatrano, R.S. (1990). A plant leucine zipper protein that recognizes an abscisic acid response element. Science *250*, 267–271.

Gupta, A., Rico-Medina, A., and Caño-Delgado, A.I. (2020). The physiology of plant responses to drought. Science *368*, 266–269.

Backman, T.W.H., and Girke, T. (2016). systemPipeR: NGS workflow and report generation environment. BMC Bioinformatics *17*, 388.

Haga, N., Kobayashi, K., Suzuki, T., Maeo, K., Kubo, M., Ohtani, M., Mitsuda, N., Demura, T., Nakamura, K., Jürgens, G., et al. (2011). Mutations in MYB3R1 and MYB3R4 cause pleiotropic developmental defects and preferential down-regulation of multiple G2/M-specific genes in Arabidopsis. Plant Physiol. *157*, 706–717.

Hayakawa, T., Hopkins, L., Peat, L.J., Yamaya, T., and Tobin, A.K. (1999). Quantitative intercellular localization of NADH-dependent glutamate synthase protein in different types of root cells in rice plants. Plant Physiol. *119*, 409–416.

Hosmani, P.S., Kamiya, T., Danku, J., Naseer, S., Geldner, N., Guerinot, M.L., and Salt, D.E. (2013). Dirigent domain-containing protein is part of the machinery required for formation of the lignin-based Casparian strip in the root. Proc. Natl. Acad. Sci. USA *110*, 14498–14503.

Ishimaru, Y., Suzuki, M., Tsukamoto, T., Suzuki, K., Nakazono, M., Kobayashi, T., Wada, Y., Watanabe, S., Matsuhashi, S., Takahashi, M., et al. (2006). Rice plants take up iron as an Fe^{3+}-phytosiderophore and as Fe^{2+}. Plant J. *45*, 335–346.

Iyer-Pascuzzi, A.S., Jackson, T., Cui, H., Petricka, J.J., Busch, W., Tsukagoshi, H., and Benfey, P.N. (2011). Cell identity regulators link development and stress responses in the Arabidopsis root. Dev. Cell *21*, 770–782.

Jin, R., Klasfeld, S., Zhu, Y., Fernandez Garcia, M., Xiao, J., Han, S.-K., Konkol, A., and Wagner, D. (2021). LEAFY is a pioneer transcription factor and licenses cell reprogramming to floral fate. Nat. Commun. *12*, 626.

Juntawong, P., Girke, T., Bazin, J., and Bailey-Serres, J. (2014). Translational dynamics revealed by genome-wide profiling of ribosome footprints in Arabidopsis. Proc. Natl. Acad. Sci. USA *111*, E203–E212.

Kadam, N.N., Tamilselvan, A., Lawas, L.M.F., Quinones, C., Bahuguna, R.N., Thomson, M.J., Dingkuhn, M., Muthurajan, R., Struik, P.C., Yin, X., et al. (2017). Genetic control of plasticity in root morphology and anatomy of rice in response to water deficit. Plant Physiol. *174*, 2302–2315.

Kadota, K., Ye, J., Nakai, Y., Terada, T., and Shimizu, K. (2006). ROKU: a novel method for identification of tissue-specific genes. BMC Bioinformatics *7*, 294.

Kajala, K., Gouran, M., Shaar-Moshe, L., Mason, G.A., Rodriguez-Medina, J., Kawa, D., Pauluzzi, G., Reynoso, M., Canto-Pastor, A., Manzano, C., et al. (2021). Innovation, conservation, and repurposing of gene function in root cell type development. Cell *184*, 3333–3348.e19.

Kamiya, T., Borghi, M., Wang, P., Danku, J.M.C., Kalmbach, L., Hosmani, P.S., Naseer, S., Fujiwara, T., Geldner, N., and Salt, D.E. (2015). The MYB36 transcription factor orchestrates Casparian strip formation. Proc. Natl. Acad. Sci. USA *112*, 10533–10538.

Katoh, K., and Standley, D.M. (2013). MAFFT mutiple sequence alignment software version 7: improvements in performance and usability. Mol. Biol. Evol. *30*, 772–780.

Kobayashi, K., Suzuki, T., Iwata, E., Nakamichi, N., Suzuki, T., Chen, P., Ohtani, M., Ishida, T., Hosoya, H., Müller, S., et al. (2015). Transcriptional repression by MYB3R proteins regulates plant organ growth. EMBO J. *34*, 1992–2007.

Konishi, N., and Ma, J.F. (2021). Three polarly localized ammonium transporter 1 members are cooperatively responsible for ammonium uptake in rice under low ammonium condition. New Phytol. *232*, 1778–1792.

Kotogány, E., Dudits, D., Horváth, G.V., and Ayaydin, F. (2010). A rapid and robust assay for detection of S-phase cell cycle progression in plant cells and tissues by using ethynyl deoxyuridine. Plant Methods *6*, 5.

Lai, X., Blanc-Mathieu, R., Grandvuillemin, L., Huang, Y., Stigliani, A., Lucas, J., Thévenon, E., Loue-Manifel, J., Turchi, L., Daher, H., et al. (2021). The LEAFY floral regulator displays pioneer transcription factor properties. Mol. Plant *14*, 829–837.

Lambert, S.A., Yang, A.W.H., Sasse, A., Cowley, G., Albu, M., Caddick, M.X., Morris, Q.D., Weirauch, M.T., and Hughes, T.R. (2019). Similarity regression predicts evolution of transcription factor sequence specificity. Nat. Genet. *51*, 981–989.

Lashbrooke, J., Cohen, H., Levy-Samocha, D., Tzfadia, O., Panizel, I., Zeisler, V., Massalha, H., Stern, A., Trainotti, L., Schreiber, L., et al. (2016). MYB107 and MYB9 homologs regulate suberin deposition in angiosperms. Plant Cell *28*, 2097–2116.

Lorbiecke, R., and Sauter, M. (1999). Adventitious root growth and cell-cycle induction in deepwater rice. Plant Physiol. *119*, 21–30.

Lucob-Agustin, N., Kawai, T., Kano-Nakata, M., Suralta, R.R., Niones, J.M., Hasegawa, T., Inari-Ikeda, M., Yamauchi, A., and Inukai, Y. (2021). Morpho-physiological and molecular mechanisms of phenotypic root plasticity for rice adaptation to water stress conditions. Breed. Sci. *71*, 20–29.

Maechler, M. (2021). cluster: "finding groups in data": cluster analysis extended Rousseeuw et al. https://CRAN.R-project.org/package=cluster.

Magyar, Z., Bögre, L., and Ito, M. (2016). DREAMs make plant cells to cycle or to become quiescent. Curr. Opin. Plant Biol. *34*, 100–106.

Maher, K.A., Bajic, M., Kajala, K., Reynoso, M., Pauluzzi, G., West, D.A., Zumstein, K., Woodhouse, M., Bubb, K., Dorrity, M.W., et al. (2018). Profiling of accessible chromatin regions across multiple plant species and cell types reveals common gene regulatory principles and new control modules. Plant Cell *30*, 15–36.

Marand, A.P., Chen, Z., Gallavotti, A., and Schmitz, R.J. (2021). A *cis*-regulatory atlas in maize at single-cell resolution. Cell *184*, 3041–3055.e21.

Meguro, A., and Sato, Y. (2014). Salicylic acid antagonizes abscisic acid inhibition of shoot growth and cell cycle progression in rice. Sci. Rep. *4*, 4555.

Mickelbart, M.V., Hasegawa, P.M., and Bailey-Serres, J. (2015). Genetic mechanisms of abiotic stress tolerance that translate to crop yield stability. Nat. Rev. Genet. *16*, 237–251.

Miyashima, S., Roszak, P., Sevilem, I., Toyokura, K., Blob, B., Heo, J.O., Mellor, N., Help-Rinta-Rahko, H., Otero, S., Smet, W., et al. (2019). Mobile PEAR transcription factors integrate positional cues to prime cambial growth. Nature *565*, 490–494.

Molina, I., Li-Beisson, Y., Beisson, F., Ohlrogge, J.B., and Pollard, M. (2009). Identification of an Arabidopsis feruloyl-coenzyme A transferase required for suberin synthesis. Plant Physiol. *151*, 1317–1328.

Mustroph, A., Juntawong, P., and Bailey-Serres, J. (2009b). Isolation of plant polysomal mRNA by differential centrifugation and ribosome immunopurification methods. Methods Mol. Biol. *553*, 109–126.

Mustroph, A., Zanetti, M.E., Jang, C.J.H., Holtan, H.E., Repetti, P.P., Galbraith, D.W., Girke, T., and Bailey-Serres, J. (2009a). Profiling translatomes of discrete cell populations resolves altered cellular priorities during hypoxia in Arabidopsis. Proc. Natl. Acad. Sci. USA *106*, 18843–18848.

Nagai, K., Mori, Y., Ishikawa, S., Furuta, T., Gamuyao, R., Niimi, Y., Hobo, T., Fukuda, M., Kojima, M., Takebayashi, Y., et al. (2020). Antagonistic regulation of the gibberellic acid response during stem growth in rice. Nature *584*, 109–114.

Nepusz, T., Yu, H., and Paccanaro, A. (2012). Detecting overlapping protein complexes in protein-protein interaction networks. Nat. Methods *9*, 471–472.

Niones, J.M., Suralta, R.R., Inukai, Y., and Yamauchi, A. (2013). Roles of root aerenchyma development and its associated QTL in dry matter production under transient moisture stress in rice. Plant Prod. Sci. *16*, 205–216.

Obertello, M., Shrivastava, S., Katari, M.S., and Coruzzi, G.M. (2015). Cross-species network analysis uncovers conserved nitrogen-regulated network modules in rice. Plant Physiol. *168*, 1830–1843.

Ogawa, D., Abe, K., Miyao, A., Kojima, M., Sakakibara, H., Mizutani, M., Morita, H., Toda, Y., Hobo, T., Sato, Y., et al. (2011). RSS1 regulates the cell cycle and maintains meristematic activity under stress conditions in rice. Nat. Commun. *2*, 278.

Ogo, Y., Itai, R.N., Kobayashi, T., Aung, M.S., Nakanishi, H., and Nishizawa, N.K. (2011). OsIRO2 is responsible for iron utilization in rice and improves growth and yield in calcareous soil. Plant Mol. Biol. *75*, 593–605.

Ogo, Y., Itai, R.N., Nakanishi, H., Inoue, H., Kobayashi, T., Suzuki, M., Takahashi, M., Mori, S., and Nishizawa, N.K. (2006). Isolation and characterization of IRO2, a novel iron-regulated bHLH transcription factor in graminaceous plants. J. Exp. Bot. *57*, 2867–2878.

Orlando, D.A., Brady, S.M., Koch, J.D., Dinneny, J.R., and Benfey, P.N. (2009). Manipulating large-scale Arabidopsis microarray expression data: identifying dominant expression patterns and biological process enrichment. Methods Mol. Biol. *553*, 57–77.

Ortiz-Ramírez, C., Guillotin, B., Xu, X., Rahni, R., Zhang, S., Yan, Z., Coqueiro Dias Araujo, P., Demesa-Arevalo, E., Lee, L., Van Eck, J., et al. (2021). Ground tissue circuitry regulates organ complexity in maize and Setaria. Science *374*, 1247–1252.

Peres, A., Churchman, M.L., Hariharan, S., Himanen, K., Verkest, A., Vandepoele, K., Magyar, Z., Hatzfeld, Y., Van Der Schueren, E., Beemster, G.T.S., et al. (2007). Novel plant-specific cyclin-dependent kinase inhibitors induced by biotic and abiotic stresses. J. Biol. Chem. *282*, 25588–25596.

Plant Cell Atlas Consortium, Jha, S.G., Borowsky, A.T., Cole, B.J., Fahlgren, N., Farmer, A., Huang, S.-S.C., Karia, P., Libault, M., Provart, N.J., et al. (2021). Vision, challenges and opportunities for a plant cell Atlas. Elife *10*, e66877.

Rambaut, A., and Drummond, A.J. (2016). FigTree v1.4 (Institute of Evolutionary Biology, University of Edinburgh). http://tree.bio.ed.ac.uk/software/figtree/.

Reynoso, M.A., Juntawong, P., Lancia, M., Blanco, F.A., Bailey-Serres, J., and Zanetti, M.E. (2015). Translating ribosome affinity purification (TRAP) followed by RNA sequencing technology (TRAP-SEQ) for quantitative assessment of plant translatomes. In Plant Functional Genomics: Methods and Protocols, J.M. Alonso and A.N. Stepanova, eds. (Springer), pp. 185–207.

Reynoso, M.A., Kajala, K., Bajic, M., West, D.A., Pauluzzi, G., Yao, A.I., Hatch, K., Zumstein, K., Woodhouse, M., Rodriguez-Medina, J., et al. (2019). Evolutionary flexibility in flooding response circuitry in angiosperms. Science *365*, 1291–1295.

Reynoso, M.A., Pauluzzi, G.C., Kajala, K., Cabanlit, S., Velasco, J., Bazin, J., Deal, R., Sinha, N.R., Brady, S.M., and Bailey-Serres, J. (2018). Nuclear transcriptomes at high resolution using retooled INTACT. Plant Physiol. *176*, 270–281.

Ritchie, M.E., Phipson, B., Wu, D., Hu, Y., Law, C.W., Shi, W., and Smyth, G.K. (2015). limma powers differential expression analyses for RNA-sequencing and microarray studies. Nucleic Acids Res. *43*, e47.

Rokas, A. (2011). Phylogenetic analysis of protein sequence data using the randomized axelerated maximum likelihood (RAXML) Program. Curr. Protoc. Mol. Biol. *Chapter 19* (Unit 19.11).

Sadasivam, S., and DeCaprio, J.A. (2013). The DREAM complex: master coordinator of cell cycle-dependent gene expression. Nat. Rev. Cancer *13*, 585–595.

Sallaud, C., Meynard, D., van Boxtel, J., Gay, C., Bès, M., Brizard, J.P., Larmande, P., Ortega, D., Raynal, M., Portefaix, M., et al. (2003). Highly efficient production and characterization of T-DNA plants for rice (Oryza sativa L.) functional genomics. Theor. Appl. Genet. *106*, 1396–1408.

Schlereth, A., Möller, B., Liu, W., Kientz, M., Flipse, J., Rademacher, E.H., Schmid, M., Jürgens, G., and Weijers, D. (2010). MONOPTEROS controls embryonic root initiation by regulating a mobile transcription factor. Nature *464*, 913–916.

Schmelz, E.A., Huffaker, A., Sims, J.W., Christensen, S.A., Lu, X., Okada, K., and Peters, R.J. (2014). Biosynthesis, elicitation and roles of monocot terpenoid phytoalexins. Plant J. *79*, 659–678.

Schuppler, U., He, P.H., John, P.C., and Munns, R. (1998). Effect of water stress on cell division and cell-division-cycle 2-like cell-cycle kinase activity in wheat leaves. Plant Physiol. *117*, 667–678.

Shahan, R., Nolan, T.M., and Benfey, P.N. (2021). Single-cell analysis of cell identity in the Arabidopsis root apical meristem: insights and opportunities. J. Exp. Bot. *72*, 6679–6686.

Shannon, P., Markiel, A., Ozier, O., Baliga, N.S., Wang, J.T., Ramage, D., Amin, N., Schwikowski, B., and Ideker, T. (2003). Cytoscape: a software environment for integrated models of biomolecular interaction networks. Genome Res. *13*, 2498–2504.

Shao, Y., Zhou, H.-Z., Wu, Y., Zhang, H., Lin, J., Jiang, X., He, Q., Zhu, J., Li, Y., Yu, H., et al. (2019). OsSPL3, an SBP-domain protein, regulates crown root development in rice. Plant Cell *31*, 1257–1275.

Shimotohno, A., Aki, S.S., Takahashi, N., and Umeda, M. (2021). Regulation of the plant cell cycle in response to hormones and the environment. Annu. Rev. Plant Biol. *72*, 273–296.

Shimura, K., Okada, A., Okada, K., Jikumaru, Y., Ko, K.-W., Toyomasu, T., Sassa, T., Hasegawa, M., Kodama, O., Shibuya, N., et al. (2007). Identification of a biosynthetic gene cluster in rice for momilactones. J. Biol. Chem. *282*, 34013–34018.

Shiono, K., Ando, M., Nishiuchi, S., Takahashi, H., Watanabe, K., Nakamura, M., Matsuo, Y., Yasuno, N., Yamanouchi, U., Fujimoto, M., et al. (2014). RCN1/OsABCG5, an ATP-binding cassette (ABC) transporter, is required for hypodermal suberization of roots in rice (Oryza sativa). Plant J. *80*, 40–51.

Singh, S., Mackill, D.J., and Ismail, A.M. (2014). Physiological basis of tolerance to complete submergence in rice involves genetic factors in addition to the SUB1 gene. AoB Plants *6*, plu060.

Sozzani, R., Cui, H., Moreno-Risueno, M.A., Busch, W., Van Norman, J.M., Vernoux, T., Brady, S.M., Dewitte, W., Murray, J.A.H., and Benfey, P.N. (2010b). Spatiotemporal regulation of cell-cycle genes by SHORTROOT links patterning and growth. Nature *466*, 128–132.

Sozzani, R., Maggio, C., Giordo, R., Umana, E., Ascencio-Ibañez, J.T., Hanley-Bowdoin, L., Bergounioux, C., Cella, R., and Albani, D. (2010a). The E2FD/DEL2 factor is a component of a regulatory network controlling cell proliferation and development in Arabidopsis. Plant Mol. Biol. *72*, 381–395.

Stamatakis, A. (2014). RAxML version 8: a tool for phylogenetic analysis and post-analysis of large phylogenies. Bioinformatics *30*, 1312–1313.

Su, S., Law, C.W., Ah-Cann, C., Asselin-Labat, M.-L., Blewitt, M.E., and Ritchie, M.E. (2017). Glimma: interactive graphics for gene expression analysis. Bioinformatics *33*, 2050–2052.

Swaminathan, S., Morrone, D., Wang, Q., Fulton, D.B., and Peters, R.J. (2009). CYP76M7 is an ent-cassadiene C11alpha-hydroxylase defining a second multifunctional diterpenoid biosynthetic gene cluster in rice. Plant Cell *21*, 3315–3325.

Terzano, R., Alfeld, M., Janssens, K., Vekemans, B., Schoonjans, T., Vincze, L., Tomasi, N., Pinton, R., and Cesco, S. (2013). Spatially resolved (semi)quantitative determination of iron (Fe) in plants by means of synchrotron micro X-ray fluorescence. Anal. Bioanal. Chem. *405*, 3341–3350.

Townsley, B.T., Covington, M.F., Ichihashi, Y., Zumstein, K., and Sinha, N.R. (2015). BrAD-seq: breath Adapter Directional sequencing: a streamlined, ultra-simple and fast library preparation protocol for strand specific mRNA library construction. Front. Plant Sci. *6*, 366.

Uga, Y., Sugimoto, K., Ogawa, S., Rane, J., Ishitani, M., Hara, N., Kitomi, Y., Inukai, Y., Ono, K., Kanno, N., et al. (2013). Control of root system architecture by DEEPER ROOTING 1 increases rice yield under drought conditions. Nat. Genet. *45*, 1097–1102.

Ursache, R., De Jesus Vieira Teixeira, C., Dénervaud Tendon, V., Gully, K., De Bellis, D., Schmid-Siegert, E., Grube Andersen, T., Shekhar, V., Calderon, S., Pradervand, S., et al. (2021). GDSL-domain proteins have key roles in suberin polymerization and degradation. Nat. Plants *7*, 353–364.

Vishwanath, S.J., Delude, C., Domergue, F., and Rowland, O. (2015). Suberin: biosynthesis, regulation, and polymer assembly of a protective extracellular barrier. Plant Cell Rep. *34*, 573–586.

Vlieghe, K., Boudolf, V., Beemster, G.T.S., Maes, S., Magyar, Z., Atanassova, A., de Almeida Engler, J., De Groodt, R., Inzé, D., and De Veylder, L. (2005). The DP-E2F-like gene DEL1 controls the endocycle in *Arabidopsis thaliana*. Curr. Biol. *15*, 59–63.

Voesenek, L.A.C.J., and Bailey-Serres, J. (2015). Flood adaptive traits and processes: an overview. New Phytol. *206*, 57–73.

Wang, W., Sijacic, P., Xu, P., Lian, H., and Liu, Z. (2018). Arabidopsis TSO1 and MYB3R1 form a regulatory module to coordinate cell proliferation with differentiation in shoot and root. Proc. Natl. Acad. Sci. USA *115*, E3045–E3054.

Wang, W., Ye, J., Ma, Y., Wang, T., Shou, H., and Zheng, L. (2020). OsIRO3 plays an essential role in iron deficiency responses and regulates iron homeostasis in rice. Plants (Basel) *9*, 1095.

Wang, Y., Huan, Q., Li, K., and Qian, W. (2021). Single-cell transcriptome atlas of the leaf and root of rice seedlings. J. Genet. Genomics *48*, 881–898.

Watanabe, Y., Kabuki, T., Kakehashi, T., Kano-Nakata, M., Mitsuya, S., and Yamauchi, A. (2020). Morphological and histological differences among three types of component roots and their differential contribution to water uptake in the rice root system. Plant Prod. Sci. *23*, 191–201.

Weirauch, M.T., Yang, A., Albu, M., Cote, A.G., Montenegro-Montero, A., Drewe, P., Najafabadi, H.S., Lambert, S.A., Mann, I., Cook, K., et al. (2014). Determination and inference of eukaryotic transcription factor sequence specificity. Cell *158*, 1431–1443.

Wisecaver, J.H., Borowsky, A.T., Tzin, V., Jander, G., Kliebenstein, D.J., and Rokas, A. (2017). A global Coexpression network approach for connecting genes to specialized metabolic pathways in plants. Plant Cell *29*, 944–959.

Won, S.-K., Choi, S.-B., Kumari, S., Cho, M., Lee, S.H., and Cho, H.-T. (2010). Root hair-specific EXPANSIN B genes have been selected for Graminaceae root hairs. Mol. Cells *30*, 369–376.

Xu, L., Naylor, D., Dong, Z., Simmons, T., Pierroz, G., Hixson, K.K., Kim, Y.-M., Zink, E.M., Engbrecht, K.M., Wang, Y., et al. (2018). Drought delays development of the sorghum root microbiome and enriches for monoderm bacteria. Proc. Natl. Acad. Sci. USA *115*, E4284–E4293.

Xuan, W., De Gernier, H., and Beeckman, T. (2020). The dynamic nature and regulation of the root clock. Development *147*, dev181446.

Yamauchi, T., Colmer, T.D., Pedersen, O., and Nakazono, M. (2018). Regulation of root traits for internal aeration and tolerance to soil waterlogging-flooding stress. Plant Physiol. *176*, 1118–1130.

Yang, M., Zhang, W., Dong, H., Zhang, Y., Lv, K., Wang, D., and Lian, X. (2013). OsNRAMP3 is a vascular bundles-specific manganese transporter that is responsible for manganese distribution in rice. PLoS One *8*, e83990.

Yeung, E., Bailey-Serres, J., and Sasidharan, R. (2019). After the Deluge: plant revival post-flooding. Trends Plant Sci. *24*, 443–454.

Zaret, K.S., and Carroll, J.S. (2011). Pioneer transcription factors: establishing competence for gene expression. Genes Dev. *25*, 2227–2241.

Zhang, H., Li, Y., Yao, X., Liang, G., and Yu, D. (2017). POSITIVE REGULATOR OF IRON HOMEOSTASIS1, OsPRI1, facilitates iron homeostasis. Plant Physiol. *175*, 543–554.

Zhang, J., Hayes, J., Zhang, L., Yang, B., Frommer, W., Bailey-Serres, J., and Girke, T. (2020). spatialHeatmap: spatialHeatmap. R package version 1.2.0. https://github.com/jianhaizhang/spatialHeatmap.

Zhang, K., Wang, M., Zhao, Y., and Wang, W. (2019a). Taiji: system-level identification of key transcription factors reveals transcriptional waves in mouse embryonic development. Sci. Adv. *5*, eaav3262.

Zhang, S., Haider, I., Kohlen, W., Jiang, L., Bouwmeester, H., Meijer, A.H., Schluepmann, H., Liu, C.-M., and Ouwerkerk, P.B.F. (2012). Function of the HD-Zip I gene Oshox22 in ABA-mediated drought and salt tolerances in rice. Plant Mol. Biol. *80*, 571–585.

Zhang, T.-Q., Chen, Y., Liu, Y., Lin, W.-H., and Wang, J.-W. (2021). Single-cell transcriptome atlas and chromatin accessibility landscape reveal differentiation trajectories in the rice root. Nat. Commun. *12*, 2053.

Zhang, Y., Yang, M., Duncan, S., Yang, X., Abdelhamid, M.A.S., Huang, L., Zhang, H., Benfey, P.N., Waller, Z.A.E., and Ding, Y. (2019b). G-quadruplex structures trigger RNA phase separation. Nucleic Acids Res. *47*, 11746–11754.

Zhao, D., Hamilton, J.P., Hardigan, M., Yin, D., He, T., Vaillancourt, B., Reynoso, M., Pauluzzi, G., Funkhouser, S., Cui, Y., et al. (2017). Analysis of ribosome-associated mRNAs in rice reveals the importance of transcript size and GC Content in translation. G3 (Bethesda) *7*, 203–219.

Zhu, L.J., Gazin, C., Lawson, N.D., Pagès, H., Lin, S.M., Lapointe, D.S., and Green, M.R. (2010). ChIPpeakAnno: a Bioconductor package to annotate ChIP-seq and ChIP-chip data. BMC Bioinformatics *11*, 237.

STAR★METHODS

KEY RESOURCES TABLE

REAGENT or RESOURCE	SOURCE	IDENTIFIER
Antibodies		
Monoclonal ANTI-FLAG_ M2 antibody produced in mouse	Sigma-Aldrich	Catalog # F1804; RRID: AB_262044
Bacterial and virus strains		
Agrobacterium tumefaciens	Plant transformation research center, UC Riverside	Strain EHA105A
Chemicals, peptides, and recombinant proteins		
M-280 streptavidin-coated Dynabeads	Thermo-Fisher Scientific	Catalog # 11205D
Fluorol yellow	Santa Cruz Biotech	Catalog # sc-215052
Click-iT EdU Cell Proliferation Kit for Imaging, Alexa Fluor 488 dye	Thermo-Fisher Scientific	Catalog # C10337
Critical commercial assays		
Nextera DNA library kit	Illumina	Catalog# FC-121-1030
pENTR-D/TOPO cloning kit	Thermo-Fisher Scientific	Catalog # K240020
LR Clonase II Enzyme mix	Thermo-Fisher Scientific	Catalog # 11791020
Deposited data		
Rice TRAP plate data	Kajala et al., 2021	NCBI: GSE149217
Rice polyA and TRAP Greenhouse and Field data	This study	NCBI: GSE180100
Rice INTACT:ATAC Greenhouse and Field data	This study	NCBI: GSE180100
Experimental models: Organisms/strains		
O. sativa: 35S TRAP	Kajala et al., 2021	Line TRAP_C_3
O. sativa: OsRSS1 TRAP	Kajala et al., 2021	Lines 57.7.2, 57.9.1,57.25,57.26
O. sativa: OsCMZ TRAP	Kajala et al., 2021	Lines 66_6_2, 66_2_4
O. sativa: AtSCR TRAP	Kajala et al., 2021	Line 46_19_2
O. sativa: OsSHR1 TRAP	Kajala et al., 2021	Lines 24_5_21, 24_5_22, 24_5_23
O. sativa: OsQHB TRAP	This study	Line 12-7-20
O. sativa: OsLSI1 TRAP	This study	Line 37-3-27
O. sativa: OsEXPB5 TRAP	This study	Line 40.5.1
O. sativa: OsNRAMP3 TRAP	This study	Line 63.7
O. sativa: OsCASP3 TRAP	This study	Lines 72.3.1, 72.2.4, 72.21
O. sativa: OsHMA5 TRAP	This study	Line 38.5
O. sativa: 35S NTF2	Reynoso et al., 2018	Lines 76.6.2, 76.7.1, 76.7.2
O. sativa: OsQHB NTF	This study	Line 68.19.3
O. sativa: OsCMZ NTF	This study	Lines 67.2.2, 67.6.3.1
Oligonucleotides		
See Table S1	This study	N/A
Recombinant DNA		
Plasmid: pH7WG-OsNTF2	Reynoso et al., 2018	N/A
Plasmid: pH7WG-OsNTF	Reynoso et al., 2018	N/A
Plasmid: pH7WG-OsTRAP	Kajala et al., 2021	N/A
Plasmid: pHGWFS7-GUS	This study	N/A
Software and algorithms		
Code used is freely available on github	This study	https://github.com/plant-plasticity/rice-root-response-atlas

RESOURCE AVAILABILITY

Lead contact

Further information and requests for resources and reagents should be directed to and will be fulfilled by the lead contact Julia Bailey-Serres (serres@ucr.edu)

Materials availability

Newly generated transgenic rice lines and plasmids are available upon completion of an MTA by correspondence with the lead contact.

Data and code availability

Rice translatome abundance data can be viewed for individual genes and groups of genes for the cell population and environmental condition comparisons in a spatialHeatMap: http://spatialheatmap.baileyserreslab.org/ ATAC-seq and RNA-seq tracks can be viewed in a JBrowse instance: http://ricejbrowse.baileyserreslab.org/ The raw TRAP and polyA RNA-seq and genomic DNA-based ATAC-seq data reported in this paper are available at NCBI GEO: GSE180100.

Code used for analyses is available at github: https://github.com/plant-plasticity/rice-root-response-atlas

EXPERIMENTAL MODEL AND SUBJECT DETAILS

Rice genetic material

Rice (*Oryza sativa cv. japonica*, Nipponbare) was used. Previously reported INTACT destination vectors (Reynoso et al., 2018) were used to construct *p35S:INTACT* BLRP-eGFP-OsWIP2/pH7WG-OsNTF2, as well as *pCMZ:INTACT* and *pQHB:INTACT* OsWPP-GFP-BLRP/pH7WG-OsNTF1. *Promoter:TRAP* constructs were prepared with the TRAP destination vector pH7WG-OsTRAP that was generated by modification of p35S:HF-OsRPL18 (Zhao et al., 2017). In this vector, the Gateway recombination site for promoter insertion is followed by a chimeric ribosomal protein consisting of a 6xHis-FLAG-3xGly tag, GFP and OsRPL18/eL18 (*OS03G0341100*). The promoters detailed in Tables S1A and S1C were recombined into pENTR-D/TOPO (Invitrogen) and introduced into the INTACT and TRAP vectors by use of LR Clonase II Enzyme mix (Invitrogen). Constructs were confirmed by Sanger sequencing. To enable promoter domain expression analysis by ß-glucuronidase (GUS) staining of tissue, promoters were cloned upstream of the *uidA* gene of *E. coli* using the vector pHGWFS7 (https://gateway.psb.ugent.be/search). T-DNA plasmids were transformed into *O. sativa japonica* cv. Nipponbare embryogenic calli, derived from mature seed embryos, by use of *Agrobacterium tumefaciens* (EHA105A) as described by Reynoso et al. (2018) and Sallaud et al. (2003) or at the UC Davis Plant Transformation Facility. Hygromycin-resistant regenerated plantlets were transferred to pots filled with Profile® Greens Grade™ in a greenhouse and grown (28°C day / 20°C night under natural light conditions) at the University of California, Riverside and allowed to self-pollinate.

Regional and cell population specificity of promoters regulating the GFP-containing INTACT and TRAP transgenes were imaged by laser scanning microscopy using a confocal Leica SP5 with a 488 nm excitation laser at 50% power, a 56.7 μm pinhole, and 650-1000 smart gain. Alternatively, a Zeiss 880 Inverted with Airyscan was used with 488 and 561 excitation laser in Lambda mode for linear unmixing to deconvolute GFP signal from autofluorescence. Brightfield images were obtained to visualize root anatomy. Promoters regulating *uidA* were evaluated by GUS staining of tissue or tissue sections and subsequent brightfield imaging. Promoter evaluation was performed on seedlings grown on sterile agar and in pots cultivated in the greenhouse as described below.

Rice growth conditions and stress treatments

For plants used for bulking of seed or stress treatments in the greenhouse, seeds were imbibed for 2 d in 5% (v/v) Liquid Smoke™ (Colgin) at 28° C in darkness to promote consistent germination. The seeds were then rinsed with distilled water and returned to 28° C in darkness for 24 h. Twenty one germinated seeds were transferred to pots (15 cm diameter and 18 cm height), filled with Profile® Greens Grade™ and placed in a greenhouse at the University of California, Riverside California during June and July 2016. The temperature was controlled at 28° C for 16 h per day and at 25° C for 8 h per night. Pots were placed in trays and watered daily with fresh water (depth of 1 cm water tray). After 10 d of growth, irrigation was switched to fertilizer water (Peters® Excel: 21-5-20 at 100 ppm N). Each pot contained 21 plants (combined as a single replicate). The location of each pot was randomized in multiple trays/tanks. After 21 d of development (from imbibition), when plants were at the V4 to V5 growth stage, four water regimes were applied. For water-sufficiency (control), pots were maintained by daily irrigation with fertilized water with drainage. For water deficit, pots were removed from the tray and watering was stopped. For waterlogging, pots were placed in tanks (56-qt clear storage box; Sterilite® 1659) and flooded with water to 2-3 cm above the root/shoot junction. For submergence, pots were transferred to tanks (grey plastic Rubbermaid® FG265500 containers) at solar midday and fully submerged with water, with the flood line 70 cm above the root/shoot junction. The containers were covered with two layers of shade cloth (SHANS 90% UV Block). A fiber optic oxygen meter (Neofox Sport, Ocean Optics, Dunedin, USA) was used to determine the percentage of dissolved oxygen in the submergence tanks in four replicates, measured at the start and end of the experiment. Oxygen content was stable at 18.90 ± 0.03% at the start (0 d) and end of the experiment (Table S1). The submergence experiment was completed independently one week following the water deficit and waterlogging experiments and therefore has its own independent control condition, totaling ten environments profiled. Five days after treatments commenced, control, submerged, or waterlogged plants were harvested or returned to normal watering conditions at midday for 24 h

before harvesting (recovery). Harvesting began one hour before subjective noon and took four to five hours for a team to complete sampling.

Plants exposed to water deficit were harvested on day five or six, depending on the leaf relative water content (RWC) determined the prior day for control and stressed plants that were not harvested for tissue. Leaf three was removed at the base of the plant and fresh, turgid, and dry weights were determined (Fukao et al., 2011). RWC was calculated as [(fresh weight – dry weight) / (turgid weight – dry weight)] × 100. RWC was also assessed for harvested control and water deficit stress plants on the day of harvest. On day four at midday, leaf RWC of water-deprived plants reached 72.9 ± 4.2%. On day five (at harvest) the RWC of well-watered plants was 95.2 ± 3.9% (Table S1). Total shoot elongation and root biomass were determined. Biological replicates were produced on separate consecutive days. Whole root systems were harvested in five independent replicates by rapid immersion in liquid nitrogen and kept at -80°C until processing.

For the field study, seedlings were germinated in Magenta boxes on selective medium after sterilization, transferred to Profile®, and grown for twelve days in the greenhouse before transplantation into a paddy maintained at eight to ten cm depth for 35 days. Planting of genotypes was based on a randomized design with ten plants per biological replicate per genotype. The genotype of each plant was confirmed after planting. The Agricultural Operations field at the University of California, Riverside Agricultural Experiment Station was prepared and pre-fertilized. Soil samples taken a week before harvesting in the wet paddy had elemental contents of 52.27 ± 16.77 ppm NO_3-N, 14.00 ± 0.32 Olsen-P and 97.00 ± 5.10 X-K (Table S1).

For growth on agar plates, the hull was removed and seeds were surface sterilized in 50% (v/v) bleach for 30 min, rinsed in sterile distilled water and arranged on plates (10 cm x 10 cm) containing 0.5x (w/v) Murashige and Skoog standard medium (MS), 1% (w/v) agar and 1% (w/v) sucrose. Plates were placed in a chamber with a 16 h day [110 $\mu Em^{-2}s^{-1}$] / 8 h night light cycle at 28°C/25°C day/night for seven days. Whole root systems were harvested into liquid nitrogen for five independent biological replicates.

All lines used to evaluate each condition were tested in the same experiment.

METHOD DETAILS

INTACT and ATAC-seq

Nuclei were purified from frozen and pulverized tissue as described previously for rice by Reynoso et al. (2019) according to the methods of Deal and Henikoff (2010) and Maher et al. (2018). To reduce cellular debris, the 70 μm filtration step was replaced by a 30 μm filtration step (Celltrics) and performing the centrifugation at 1000 x *g* at 4° C for 15 min. The quantity of tissue for specific sample preparations is provided in Table S1B. Nuclei were counted prior to ATAC-seq for all lines except *pQHB:INTACT*, due to low yield. ATAC-seq was performed by Tn5 insertion into chromatin of purified nuclei using the Nextera DNA Library Preparation Kit on nuclei as described (Reynoso et al., 2019). ATAC-seq libraries were sequenced on the NextSeq 500 at the UC Davis DNA Technologies Core to obtain 36 nt paired-end reads.

TRAP and RNA-seq libraries

TRAP was performed as previously described (Mustroph et al., 2009b; Reynoso et al., 2015) with slight modifications through polyA RNA purification as described by Reynoso et al. (2019). Isolation of total RNA and the synthesis of non-directional mRNA sequencing libraries by random priming (Townsley et al., 2015) also followed prior methods (Reynoso et al., 2019). Samples included at least three biological replicates for each condition and line. Sequencing was performed with a Illumina HiSeq 3000 to obtain 50 nt single-end reads.

EdU staining and growth measurements

Seeds with seed coats removed were sterilized in 50% (v/v) bleach for 10 min followed by rinsing with ddH_2O. All growth was under a 16 h light (115 $\mu E\ m^{-2}\ s^{-1}$) / 8 h dark cycle at 22°C in a growth chamber. For submergence, each seed was planted at the top of 6 mL of moist Profile® in a 23 mL borosilicate glass tube (16 mm x 150 mm; Fisher), grown for 7 d before full submergence in ddH_2O at Zeitgeber time 6, for 24 h in darkness. For recovery, tubes were drained and returned to the chamber for 24 h. Primary roots were evaluated, as seedling crown roots were more variable in length and number. For primary root length measurements, seedlings of similar coleoptile length were fully submerged in darkness for 3 d or maintained in air under darkness for 3 d. For water deficit, seedlings were grown in pots (6 cm diameter x 6 cm height) filled with Profile®. On day 8, 50-75% of the endosperm was gently excised and plants were deprived of water for 3 d at which time leaves were rolled. Roots were sampled or rewatered and then sampled after 24 hours of recovery, with corresponding 11 d old controls for EdU staining or 12 d old controls for primary root length. Root tips were stained using the Click-iT® EdU Imaging Kit (Invitrogen) according to the manufacturer's protocol by immersion of the apical region of primary root in 100 μM EdU (5-ethynyl-2′-deoxyuridine) for 1 h and washed twice with 100 mM Tris-HCl (pH 8.0) before placement on a 1 mm thick glass microscope slide with a high precision coverslip (170 ± 5 μM thickness, Thor Labs, #1.5H) and incubation in the Click-iT EdU detection cocktail for 30 min in darkness. Root sections were washed with 100 mM Tris-HCl (pH 8.0) and immersed in 0.4 μg/μL DAPI (4′,6-diamidino-2-phenylindole) for 5 min and washed again before imaging with a Zeiss LSM 880 upright microscope. Acquisition of DAPI and EdU fluorescence was with an excitation laser of 395 and 495 nm, and gain of 544 and 800, respectively. Fluorescent signal was quantified for the elongation zone to the root apex using the combined Z stack image.

Suberin staining

Suberin was visualized after Fluorol Yellow (FY) staining. Briefly, roots were incubated in 0.01% (w/v) FY solution in lactic acid (Sigma) for 60 min, rinsed three times with distilled water, and counterstained with 0.5% (w/v) aniline blue for 5 min under vacuum, and then 25 min at room temperature in darkness. Roots were observed by Confocal Laser Scanning microscopy in a Leica SP5 using GFP settings, smart gain (800), laser at 50% and pinhole set at Airy 1. Corrected Total Cell Fluorescence (CTCF) was calculated using ImageJ as described (Clark et al., 2019). Briefly, integrated density of fluorescence is divided by the area of the cells multiplied by the mean fluorescence of a region with no signal defined as background.

Perls-DAB staining

Plants were grown in three replicates staggered by one day in a greenhouse in Riverside, CA, as described above, with five plants per pot. Water was withheld for 29 days to achieve similar dehydration levels (onset of leaf rolling) to the TRAP-seq experiments; a longer duration was required due to shorter day length and cloudy weather. Whole root systems of plants (stage V5-6) were harvested into fixation solution (MeOH, $CHCl_3$, HOAc; 6:3:1) and Fe was visualized using Perls staining followed by diaminobenzidine (DAB) intensification (Brumbarova and Ivanov, 2014). Photographs of whole root systems (n=9 for WD, n=8 for CON, 2-3 per replicate) were scored from 1 (least staining intensity) to 4 (most staining intensity) by five researchers who were blinded to the treatment and the experimental design. Crown roots (2-8 cm) were sectioned approximately 1-2 cm from the root tip by embedding in 4% (w/v) agarose and generating 100 μm sections using a EMS5000 Oscillating Tissue Slicer. Sections were imaged using the brightfield setting on a Keyence BZ-X710 Microscope with 20X magnification.

QUANTIFICATION AND STATISTICAL ANALYSIS

ATAC-seq and RNA-seq data processing

Short read processing, quality assessment, alignment to the genome were performed as described (Reynoso et al., 2019) using the University of California, Riverside Institute for Integrative Genome Biology high performance bioinformatics cluster (http://www.bioinformatics.ucr.edu/), supported by NSF MRI DBI 1429826 and NIH S10-OD016290. For these analyses, we used R packages from Bioconductor including systemPipeR (Backman and Girke, 2016) and IGRSP1.0-30 genome (http://plants.ensembl.org/Oryza_sativa/Info/Index) with the Bowtie2/Tophat2 suite. Read count data for features of exons-by-genes were obtained with the summarizeOverlaps function of GenomicRanges (Juntawong et al., 2014). For visualization of data in a genome browser, Samtools 1.0.9 was used to convert reads from SAM to sorted BAM files. ATAC Bowtie2 aligned SAM files were filtered to retain only reads with a mapping quality score of 10 or higher. BedTools 2.26 genomeCoverageBed was used to make bigwig files which were converted to UCSC bedGraphtoBigWig 332–0 files with rpkm normalization.

RNA-seq differential expression, mapping of chromatin accessibility, identification of Transposase Hypersensitive Sites, and evaluation of accessibility changes between conditions

A pipeline in R that we developed previously (Reynoso et al., 2019) was used to obtain different contrasts in mRNA abundance based on environment, including $\log_2$ Fold Change (FC) values and adjusted P values (adj.P.Val). This included use of the limma-voom Bioconductor package in R for quantile normalization and FC calculations (Ritchie et al., 2015) and production of multidimensional scaling (MDS) plots using Glimma (Su et al., 2017) using genes with more than 3 count per million in at least three biological replicates. The total number of detectable mRNAs for any given *promoter:TRAP* translatome was consistent across treatments (Table S5B), indicating translatome differences are not due to differences in library complexity. The voom function on the limma package was used to calculate normalized counts. Following normalization, count data were used to calculate transcripts per million reads (TPM). Top varying genes were analyzed for dominant patterns of coregulation as described previously (Orlando et al., 2009). Evaluation of enrichment in Gene Ontology terms was performed with systemPipeR (Backman and Girke, 2016) using rice GO definitions obtained from BioMart. To integrate *p35S* polyA and TRAP stress changes for roots, limma voom $\log_2$ FC values for DEGs in each condition ($|\log_2 FC| > 1$ and $Padj < 0.01$]) compared to control were clustered using the Partitioning Around Medoids (PAM) method with $k = 15$ clusters using gplots, cluster, e1071, and RcolorBrewer R packages. Several k values were tested for resolution of correlated genes. *p35S* ATAC $\log_2$ FC values were calculated for normalized reads located up to 2kb upstream of the ATG for genes in each cluster and median value plotted in the heatmap.

Peaks in ATAC data were found running the HOMER package function "Findpeaks" with the parameters "-minDist 150" "-region" and "-regionRes 1". THSs locations were kept if they overlapped at least by 50 bp in biological replicates of the same condition. This was done using the "findOverlapsOfPeaks" function of the ChIPPeakAnno package (Zhu et al., 2010). Reproducible peaks are referred to as THSs. The fraction of reads in peaks was calculated using the frip() function of the encodeChIPqc package. Read alignments overlapping with THSs coordinates were quantified in three biological replicates for each sample. Counts for each THSs were statistically evaluated using limma voom after quantile normalization. THSs with a $\log_2$ fold change value of more than 1, or less than -1, and adjusted p-value < 0.05 were identified as dTHSs, which refer to chromatin regions where chromatin is more accessible or less accessible between two conditions.

We developed a *spatialHeatmap* Shiny App instance to visualize the cell and tissue level gene expression data of this study interactively within the context of anatomical images from rice roots (https://github.com/jianhaizhang/spatialHeatmap) (Zhang et al., 2020).

Network construction

Coexpression networks were generated using all rice RNA-seq (TRAP and Total) data from this work and Kajala et al. (2021) as described in Wisecaver et al. (2017) using scripts from https://github.itap.purdue.edu/jwisecav/mr2mods (Data S2). Briefly, the Pearson correlation coefficient (PCC) is calculated for all possible pairs of genes based on normalized counts across all the data provided. These are used to calculate the mutual rank score (the geometric mean of the reciprocal ranks) for each pair of genes. Mutual rank scores are converted to network edge weights with five different exponential decay functions, producing five different networks with varying stringency for connections. Finally, ClusterONE is used to call modules for each of these networks (Nepusz et al., 2012).

To model gene regulatory networks and infer hierarchies, Taiji version 0.5.0 (Zhang et al., 2019a) was run on fifteen paired ATAC-seq and TRAP-seq datasets, using a.meme file generated from the CisBP database (Lambert et al., 2019), with the addition of the hypoxia-responsive promoter element (HRPE) motif reported previously (Gasch et al., 2016) assigned to *OsERF66* and *67*. To identify genes with specific activity (PageRank scores uniquely elevated in a certain cell population or condition), the output gene rank matrix was filtered to TFs with a row Z-score of at least 2.5 in at least one condition/cell population, and then clustered with partitioning around medoids (PAM) clustering in R (Maechler, 2021). These clusters were summarized using word clouds (Fellows, 2012) based on the frequency of TF Families in each cluster. To visualize networks, the network output from Taiji (Zhang et al., 2019a) was filtered to only edges where genes in the cluster are both a source and target node, then loaded into Cytoscape (Shannon et al., 2003), laid out with ''Hierarchical layout,'' and manually adjusted for spacing. Node size was assigned by PageRank score and color by TPM.

To build a cell cycle network (Figure 2C), cell cycle and DNA synthesis genes were identified from the literature. The analysis included *pRSS1* and *p35S* TRAP and *p35S* INTACT data across the nine conditions. Genes included in the network met at least one of the following criteria: a) differentially regulated in response to waterlogging, water deficit or submergence relative to the control treatment (translatomes of *p35S*, *pRSS1*-marked cells and polyA mRNA) ($|\log_2 FC|>1$ & padj<0.01); b) genes present in polyA and *p35S* TRAP cluster analysis; c) genes present in expression pattern analysis in *pRSS1* and *p35S* translatomes. To identify enriched transcription factor binding sites (TFBSs), THSs located nearby selected genes were searched for enrichment in comparison to the rest of accessible regions THSs using AME with the following parameters –hit-lo-fraction 0.01 –evalue-report-threshold 10. TFs associated with enriched TFBSs were filtered requiring at least 3 TPM in one condition. TFBSs were searched on the genome using FIMO with the following parameters –max-stored-scores 10000000000 –thresh 0.0001 as performed previously (Reynoso et al., 2019). Next, connections to targets were assigned based on the presence of TFBS inside THS located in a range from 2 kb upstream to 1kb downstream of target genes. The resulting network was overlaid with significant *pRSS1* SUB vs. CON DEG information as well as Z-scores for transcript abundance in *pRSS1* across conditions.

To build a ground tissue network, genes in Pattern 27 (Figure 3C) were processed the same way. ERF binding sites were excluded to decrease complexity and facilitate visualization as most genes in the network contained at least one ERF site, other TFs were filtered by requiring presence in the pattern except for E2F-like which was kept as TF node based on its reported presence in same complexes with OsDP1.

To develop the suberin network (Figure 4D), after testing enrichment of TFBSs in their proximal THS for the coexpression module, we searched the accessible regions 2 kb upstream or 1 kb downstream of the TSSs of module genes of enriched TFBSs that were associated with a TF that was expressed at least 10 TPM in any of the LSI1 greenhouse TRAP conditions. Additionally, we also searched for TFBSs associated with any TF Gene that was present in the coexpression module, regardless of whether or not it was enriched.

Source and target nodes were imported into Cytoscape (Shannon et al., 2003) and the NetworkAnalyzer tool in Cytoscape was used to calculate edge betweenness, and the ''Edge-weighted spring embedded layout'' was executed using edge betweenness.

Identification of Cell Population Enriched Genes (CPEGs)

ROKU (Kadota et al., 2006) was run on mean TPM values for TRAP-seq data for each *promoter:TRAP* line for which data were generated in the field, with parameters set so that a gene could only be enriched in one cell population (upper.limit =.2). These gene sets of CPEGs were tested for GO enrichment as previously described. This process was repeated independently for each condition/environment where at least three *promoter:TRAP* lines were assayed, and then these gene sets were intersected to identify environmentally conserved CPEGs for *promoter:TRAP* lines represented in at least two of three: plate, greenhouse, field experiments (*pRSS1, pLSI1, pQHB*, and *p35S*).

To generate networks, as described for cell cycle and suberin above, THSs proximal to CPEGs for each class were input into AME to test for enrichment of the CisBP motifs, with all other THSs as a negative control. Enriched motifs that were associated with TF genes that themselves were CPEGs were searched using FIMO in THSs from 2 kb upstream to 1 kb downstream of CPEG genes, and these FIMO searches were used to generate networks in Cytoscape, with ''Edge-weighted spring embedded layout" based on Edge betweenness.

Phylogeny

Gene orthology relationships for E2F/DP genes were determined following (Rokas, 2011). This was generated by downloading a hmm for the E2F_TDP family from Pfam (http://pfam.xfam.org/family/PF02319), then searching the proteomes of *Oryza sativa*, *Arabidopsis thaliana*, *Medicago truncatula*, *Solanum lycopersicum*, *Chlamydomonas reinhardtii*, *Vitis vinifera*, *Selaginella*

moellendorffii, *Homo sapiens*, and *Sorghum bicolor* for matching proteins using hmmsearch from hmmer3.3.2 (Finn et al., 2011). Next, sequences were aligned with mafft 7.471 (Katoh and Standley, 2013) using default settings, then alignment trimmed with trimal 1.4.1 (Capella-Gutiérrez et al., 2009) with -gt 0.5. Finally, a tree was generated with RAxML 8.2.12 (Stamatakis, 2014) with 100 bootstraps and -m PROTGAMMAAUTO. The resulting tree was midpoint rooted and visualized in FigTree 1.4.3 (Rambaut and Drummond, 2016).